# Spray Cooling of Steel Dies in a Hot Forging Process

by

Matthew Jason Endres

A Thesis

Submitted to the Faculty

of the

WORCESTER POLYTECHNIC INSTITUTE

in partial fulfillment of the requirements for the

Degree of Master of Science
in
Mechanical Engineering

August 30, 2002

Approved:

_____
Dr. Brian J. Savilonis, Thesis Advisor

_____
Dr. Michael Demetriou, Graduate Committee Representative

_____
Dr. David Olinger, Committee Member

_____
Dr. John Blandino, Committee Member

# Abstract

Spray cooling has been important to control die temperature in forging processes for years. One area that has had little research is how thermal stresses in a metal are related to flow characteristics of the spray. Wyman-Gordon Corporation at its North Grafton MA facility uses spray cooling to cool their die after a forging process. It is believed that the current system used causes cracking along the surface of the impression in the die. The purpose of this work is to compare the nozzle system used by Wyman-Gordon to selected commercially available spray nozzles, and determine if there is a better spray cooling system than the one currently used. First, the Sauter mean diameter, particle velocity, and volumetric spray flux were experimentally found using a laser PDA system for four water driven nozzles, including the Wyman-Gordon nozzle, and one air-atomizing nozzle. The water atomizing nozzles were tested using pressures from 30 psi to 150 psi. For the air-atomizing nozzle, the water pressure was set at 60 psi and the air pressure was varied from 30 to 150 psi. Three nozzles were chosen: the Wyman-Gordon nozzle, a smaller orifice water atomizing nozzle, an air-atomizing nozzle, and an air stream, to conduct an heat conduction experiment. Using the temperature gradients created by the cooling effects of each nozzle, the heat flux and induced thermal stresses were determined. The results showed the Wyman-Gordon nozzle was causing higher thermal stresses than the air/water and water nozzles. However, the air-atomizing nozzle and air stream, due to the high temperatures that the dies are subjected to, did not cool the die quick enough to be practical. The smaller orifice water atomizing nozzle proved to be the nozzle that would cool the surface of the dies within a practical time, and induce allowable thermal stresses, sufficiently enough below the yield strength of the die material. These results, although collected specifically to study the cooling of dies at Wyman-Gordon, could be generalized to include the cooling of any test piece with a high surface temperature.

# Spray Cooling of Steel Dies in a Hot Forging Process

by

Matthew Jason Endres

A Thesis

Submitted to the Faculty

of the

WORCESTER POLYTECHNIC INSTITUTE

in partial fulfillment of the requirements for the

Degree of Master of Science
in
Mechanical Engineering

August 30, 2002

Approved:

_____
Dr. Brian J. Savilonis, Thesis Advisor

_____
Dr. Michael Demetriou, Graduate Committee Representative

_____
Dr. David Olinger, Committee Member

_____
Dr. John Blandino, Committee Member

# Abstract

Spray cooling has been important to control die temperature in forging processes for years. One area that has had little research is how thermal stresses in a metal are related to flow characteristics of the spray. Wyman-Gordon Corporation at its North Grafton MA facility uses spray cooling to cool their die after a forging process. It is believed that the current system used causes cracking along the surface of the impression in the die. The purpose of this work is to compare the nozzle system used by Wyman-Gordon to selected commercially available spray nozzles, and determine if there is a better spray cooling system than the one currently used. First, the Sauter mean diameter, particle velocity, and volumetric spray flux were experimentally found using a laser PDA system for four water driven nozzles, including the Wyman-Gordon nozzle, and one air-atomizing nozzle. The water atomizing nozzles were tested using pressures from 30 psi to 150 psi. For the air-atomizing nozzle, the water pressure was set at 60 psi and the air pressure was varied from 30 to 150 psi. Three nozzles were chosen: the Wyman-Gordon nozzle, a smaller orifice water atomizing nozzle, an air-atomizing nozzle, and an air stream, to conduct an heat conduction experiment. Using the temperature gradients created by the cooling effects of each nozzle, the heat flux and induced thermal stresses were determined. The results showed the Wyman-Gordon nozzle was causing higher thermal stresses than the air/water and water nozzles. However, the air-atomizing nozzle and air stream, due to the high temperatures that the dies are subjected to, did not cool the die quick enough to be practical. The smaller orifice water atomizing nozzle proved to be the nozzle that would cool the surface of the dies within a practical time, and induce allowable thermal stresses, sufficiently enough below the yield strength of the die material. These results, although collected specifically to study the cooling of dies at Wyman-Gordon, could be generalized to include the cooling of any test piece with a high surface temperature.

# Acknowledgements

Many hours have gone into creating this thesis. My primary thanks go to Professor Brian Savilonis for his thorough, efficient, and ongoing suggestions and support through the thesis. I am forever in his debt.

The many contributors should also be thanked for taking the time assist me in testing. First is Matt Davy whose tireless effort allowed me to set up the PDA system. Also to San Ping Ho whose guidance was instrumental to being able run the sensitive PDA system and coordinate the spraying tests. Finally, to Bruce Sioun from the Wyman-Gordon for his whole hearted effort and his vision to improving the process at Wyman-Gordon. Every company should have a person with his drive to continual improvement.

Special thanks go to all the people at Wyman-Gordon, specifically David Kalmanovitch for their suggestions, encouragement and effort, without which I would have lost my sanity and not have finished the thesis.

# Acknowledgements

Many hours have gone into creating this thesis. My primary thanks go to Professor Brian Savilonis for his thorough, efficient, and ongoing suggestions and support through the thesis. I am forever in his debt.

The many contributors should also be thanked for taking the time assist me in testing. First is Matt Davy whose tireless effort allowed me to set up the PDA system. Also to San Ping Ho whose guidance was instrumental to being able run the sensitive PDA system and coordinate the spraying tests. Finally, to Bruce Sioun from the Wyman-Gordon for his whole hearted effort and his vision to improving the process at Wyman-Gordon. Every company should have a person with his drive to continual improvement.

Special thanks go to all the people at Wyman-Gordon, specifically David Kalmanovitch for their suggestions, encouragement and effort, without which I would have lost my sanity and not have finished the thesis.

# Table of Contents

Abstract ..... ii
Acknowledgements ..... iii
Table of Contents ..... iv
Table of Figures ..... v
1.0. Background ..... 1
1.1. Previous Research ..... 3
1.2. Heat Transfer Regimes ..... 10
1.3. Determination of Heat Flux ..... 12
1.4. Determination of Thermal Stresses ..... 13
2.0. Sensitivity and Error Analysis ..... 14
3.0. Experimental Methods and Procedure ..... 16
3.1. Spray system ..... 17
3.2. PDA System ..... 18
3.2. Heat Conduction Experiment ..... 21
4.0. Results and Discussion ..... 22
4.1. Spray Characteristics ..... 22
4.2. Heat Conduction Experiment ..... 42
5.0. Discussion and Conclusions ..... 50
6.0. Recommendations ..... 53
References ..... 54
Appendix A ..... 55
Appendix B ..... 56
Appendix C ..... 58
Appendix D ..... 60

# Table of Figures

Figure 1: Heat flux vs particle velocity for constant particle diameter and volumetric flux.... 5
Figure 2: Heat flux vs particle diameter for constant particle velocity and volumetric flux.... 6
Figure 3: Heat flux vs Volumetric flux for constant particle diameter and particle velocity... 6
Figure 4: Convective Currents in Horizontal Fluid Layer [10] ..... 10
Figure 5: The four regimes of boiling: (a) Natural convection, (b) isolated bubbles, (c) columns and slugs, (d) film boiling [11]. ..... 12
Figure 6: Schematic of Spray Setup ..... 18
Figure 7: PDA setup ..... 19
Figure 8: Thermocouple positions on 14-inch diameter by 8-inch long test piece (depth and location have the units of inches) ..... 21
Figure 9: Particle diameter as measured from the center of the spray ..... 22
Figure 10: Volumetric spray flux as a function of distance ..... 23
Figure 11: Particle velocity as measured from the center of the spray ..... 23
Figure 12: Smaller orifice average velocity results ..... 24
Figure 13: Smaller orifice volumetric spray flux results ..... 25
Figure 14: Sauter mean diameter results for smaller orifice nozzle ..... 26
Figure 15: Approximate heat flux in smaller orifice nozzle ..... 27
Figure 16: Volumetric Spray Flux results for larger orifice circular spray ..... 28
Figure 17: Average velocity results for larger orifice circular spray ..... 28
Figure 18: Manufacturer's flow rates and actual flow rates for smaller orifice nozzle ..... 29
Figure 19: Sauter mean diameter results for larger orifice circular spray ..... 30
Figure 20: Estimated heat flux results for larger orifice circular spray ..... 30
Figure 21: Manufacturer's and actual flow rates for larger orifice nozzle ..... 31
Figure 22: Average velocity results for square spray ..... 32
Figure 23: Volumetric spray flux results for square spray ..... 32
Figure 24: Sauter mean diameter results for square spray ..... 33
Figure 25: Estimated heat flux results for square spray ..... 34
Figure 26: Manufacturer's and Actual flow rates for the square spray nozzle ..... 34
Figure 27: Volumetric spray flux results for air atomizing nozzle ..... 35
Figure 28: Average velocity results for air atomizing nozzle ..... 36
Figure 29: Sauter mean diameter results for air atomizing nozzle ..... 37
Figure 30: Estimated heat flux results for air atomizing nozzle ..... 37
Figure 31: Theoretical and Actual flow rates for air-atomizing nozzle ..... 38
Figure 32: Sauter Mean Diameter variation from center of spray ..... 39
Figure 33: Average velocity variation from center of spray ..... 40
Figure 34: Cooling rates for the various nozzles ..... 42
Figure 35: Actual cooling rates ..... 43
Figure 36: Radial stress variance as a function of the distance from the surface ..... 45
Figure 37: Experimental heat flux for air-atomizing nozzle at surface (z=0), (air = 90 psi, water = 60 psi) ..... 47
Figure 38: Experimental heat flux for water atomizing nozzle (70 psi) ..... 48
Figure 39: Experimental heat flux for Wyman-Gordon nozzle ..... 49
Figure 40: Wyman-Gordon nozzle inverse heat conduction test ..... 55
Figure 41: Air-Atomizing nozzle inverse heat conduction test ..... 56

Figure 42: Air-Atomizing nozzle inverse heat conduction test (15 seconds later)..... 57
Figure 43: Water atomizing nozzle inverse heat conduction test ..... 58
Figure 44: Water atomizing inverse heat conduction test (15 seconds later) ..... 59

Nomenclature

c – Piece thickness [m]

$c_p$— Specific heat [J / kg K]

$\bar{d}$ — Droplet mean diameter [m]

E – Modulus of Elasticity

$f$ — Thermal stresses [Pa]

$h_{fg}$ — Latent heat of vaporization [J / kg]

$Q$ — Volumetric spray flux [cc / sec / $cm^2$]

$q^*$ — Dimensionless surface heat flux

r — Radius from center of test piece [m]

$RA$ — Ratio of droplet cross surface mean velocity and the volumetric spray flux

Re —Reynolds number

$T^*$ —Dimensionless surface temperature

$T_\infty$ — Fluid temperature [°C]

$t$ — Time [sec]

$\bar{u}$ — Mean droplet velocity averaged over the cross-section [m / s]

$We$ — Weber number

z – Distance parameter measured vertically [m]

$\alpha$ — Thermal diffusivity [$m^2$ / s]

$\delta$ — Piece thickness [m]

$\mu_l$, $\mu_g$ — Viscosity [kg / s m]

ν – kinematic viscosity

$\rho_l$ , $\rho_g$ —Density [kg / $m^3$]

$\sigma$ — Surface tension [N / m]

# 1.0. Background

The Wyman-Gordon process of spray cooling the die after forging is of interest. First, the dies are preheated up to 470° C (878$^{o}$ F) before being fastened to the press plates as to lessen the thermal gradients between the forging and the dies. Then the heated metal piece at temperatures up to 649°C (1200$^{o}$ F) hot metal forging is placed into the dies and pressed. After a press run has been made, the hot metal forging is removed from the die. The dies are typically at a temperature ranging from 370 to 538$^{o}$ C (700 to 1000$^{o}$ F). Then a worker proceeds to open a valve that releases the air/water mixture from a hand held nozzle to cool the dies down to an ideal operating temperature and to clean scale from the piece. The surface temperature of the die is then checked with an infrared pyrometer to make sure it is in the ideal operating temperature.

Die temperature control through spray cooling is important to a manufacturing company for numerous reasons. First, cooling ensures that the atomic structure of the die material does not change to a more brittle phase, which would have a lower resistance to wear. By controlling the overall surface temperature of the die, it is possible to obtain the desired dimensional properties of the forging and to increase the life of the die. Additionally, the surface finish, casting soundness, and quality over different areas can be controlled and improved [1]. Often the water or other liquid involved with spray cooling is used as a lubricant. Cooling and lubrication have traditionally been done with an automated spray system in combination with cooling passages or other means of heat extraction [2]. However, due to the immense die size and the numbers of moving parts associated with the

forging, cooling passages and automatic spraying systems have been proven impractical for large dies as in the Wyman-Gordon process.

Two ways of creating small water droplets for spray cooling are through air atomization and pure water atomization. In air atomization, pressurized air breaks up a stream of water into fine particles. Air atomization usually produces smaller but faster droplet sizes (around 10 to 50 micrometers and 50 to 100 m/s respectively). Pure water atomization uses forced liquid, and the internal nozzle design itself breaks up the water stream producing larger and slower particles (100 to 500 micrometers and 2 to 40 m/s) [3].

## 1.1. Previous Research

There has been little research done on air-atomization spray cooling of dies and the related thermal stresses within the material being cooled. Liu et al. [4] examines the heat transfer characteristics involved with a hot die surface. The team sprayed a hot test surface using different combinations of air/water pressures, while recording the heat flux induced on the hot surface as a function of the air/water pressure. Finally, they used a PDA system to measure the properties of the spray including the droplet size, velocity and volumetric spray flux. The range for the average velocities tested was from 5 to 25 m/s, the Sauter mean diameter ranged from 5 to 40 micrometers, the volumetric spray flux was 0.005 to 0.015 $cc/s/cm^2$, the liquid and water pressure from 1 to 4 bar, and the surface temperatures from 150 to 300° Celsius (302 F to 572 F). Their results indicated that at constant air pressure and a given surface temperature, the heat flux increases with an increase of liquid pressure, peaks, and then drops for higher liquid pressures. The same trend was found at a given surface temperature for constant water pressure and increasing air pressure. For constant water pressure, the droplet diameter decreases with an increase of air pressure, which improves the heat transfer. For both mentioned cases, the velocity increases with an increase of water pressure or air pressure over the entire test range. Their results indicated, within 2 percent, the dimensionless heat flux ($q^*$) and the dimensionless temperature ($T^*$) are given by the following equation.

$$q^* = AT^{*3} + BT^{*2} + CT^* + D \tag{1}$$

Where the values for the constants A, B, C, and D are:

$$A = 10^{-4.05434} * Re^{1.45101} * We^{1.27899} * RA^{0.864281} \quad (2)$$

$$B = -10^{-3.6164} * Re^{1.31859} * We^{1.17256} * RA^{0.915949} \quad (3)$$

$$C = 10^{-3.64182} * Re^{1.21498} * We^{1.09276} * RA^{0.949317} \quad (4)$$

$$D = -10^{-4.15201} * Re^{1.13977} * We^{1.03674} * RA^{0.963274} \quad (5)$$

Where the Reynolds number is defined as $\mathrm{Re} = \frac{\rho_l \bar{u} \bar{d}}{\mu}$, the Weber number is defined as $We = \frac{\sigma}{\rho_l \bar{u}^2 \bar{d}}$, the ratio of droplet velocity to the volumetric liquid flux is $RA = \frac{\bar{u}}{Q}$, the dimensionless heat flux is $q^* = \frac{q}{\rho Q h_{fg}}$, and the dimensionless temperature is $T^* = \frac{T_{sur} C_p}{h_{fg}}$.

By plotting the three variables: particle velocity, diameter, and volumetric spray flux, versus the heat flux q, one can determine the most dominant term based upon how much the heat flux is affected by a change in the parameter. For instance, in Figure 1, the particle diameter and volumetric flux are set as constants, and the particle velocity is plotted over the entire tested range. This is then repeated for the other two parameters, Sauter mean particle diameter (Figure 2) and volumetric spray flux (Figure 3). Although all three seem to have an effect over the entire range, upon closer inspection, one can observe that the change in the heat flux versus the change in the parameter is highest for the volumetric spray flux, followed by diameter and velocity. The dependence of heat flux on volumetric spray flux indicates that the heat flux is most sensitive to changes in the volumetric spray flux. To quantify these results, the change in the heat flux (delta y) is divided by the change in the parameter (delta x) and reported as an overall percent change in the heat flux. The results of

this calculation are as follows: $\frac{\Delta q}{\Delta u} = 1.94\%$, $\frac{\Delta q}{\Delta d} = 4\%$, and $\frac{\Delta q}{\Delta Q} = 9\%$. The sensitivity for the volumetric spray flux more than twice as high as the Sauter mean diameter.

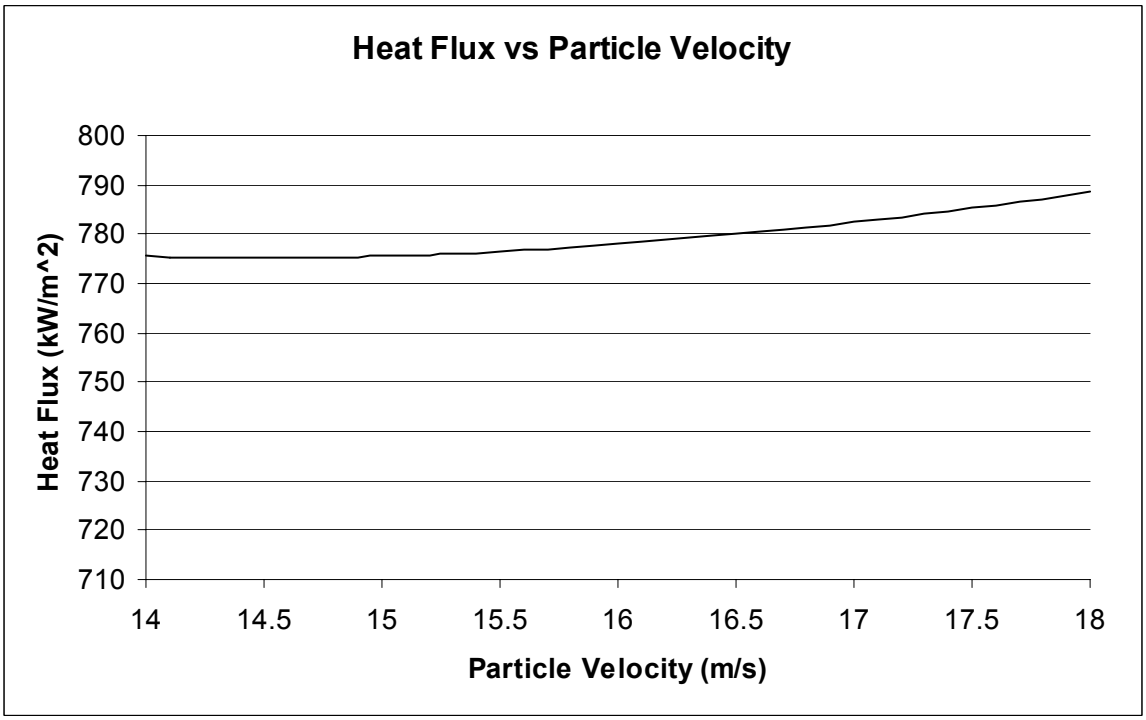


**Figure 1: Heat flux vs particle velocity for constant particle diameter and volumetric flux.**

These data based on Liu et al [2].

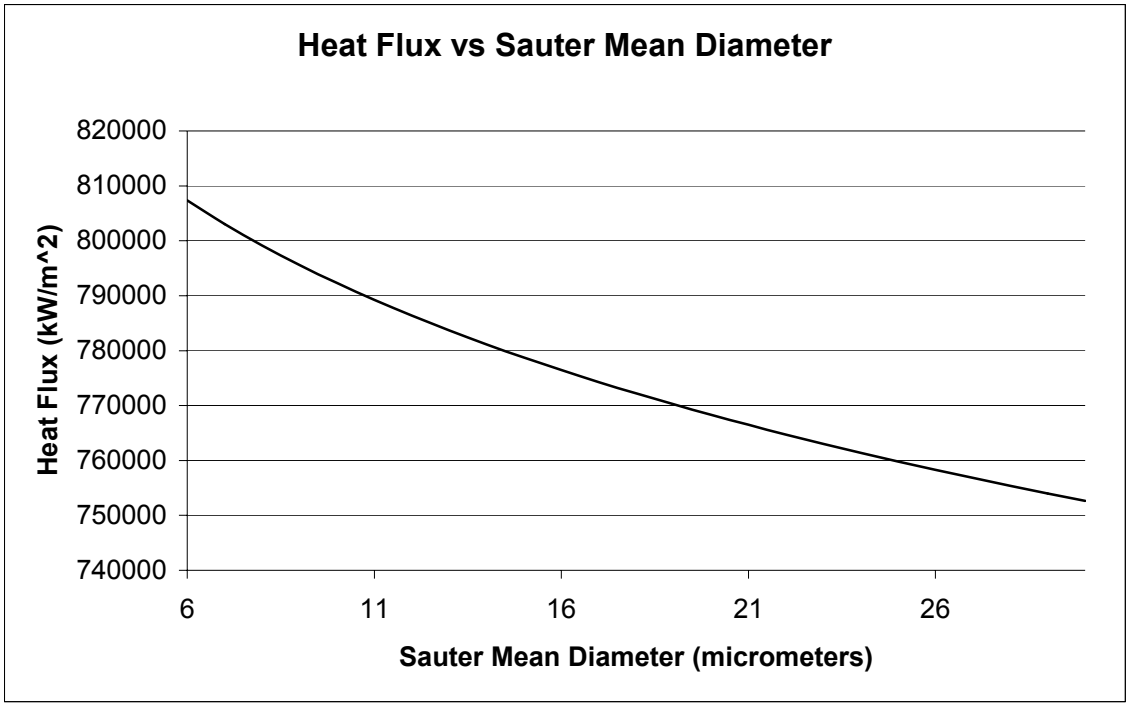


**Figure 2: Heat flux vs particle diameter for constant particle velocity and volumetric flux.**

These data based on Liu et al [2].

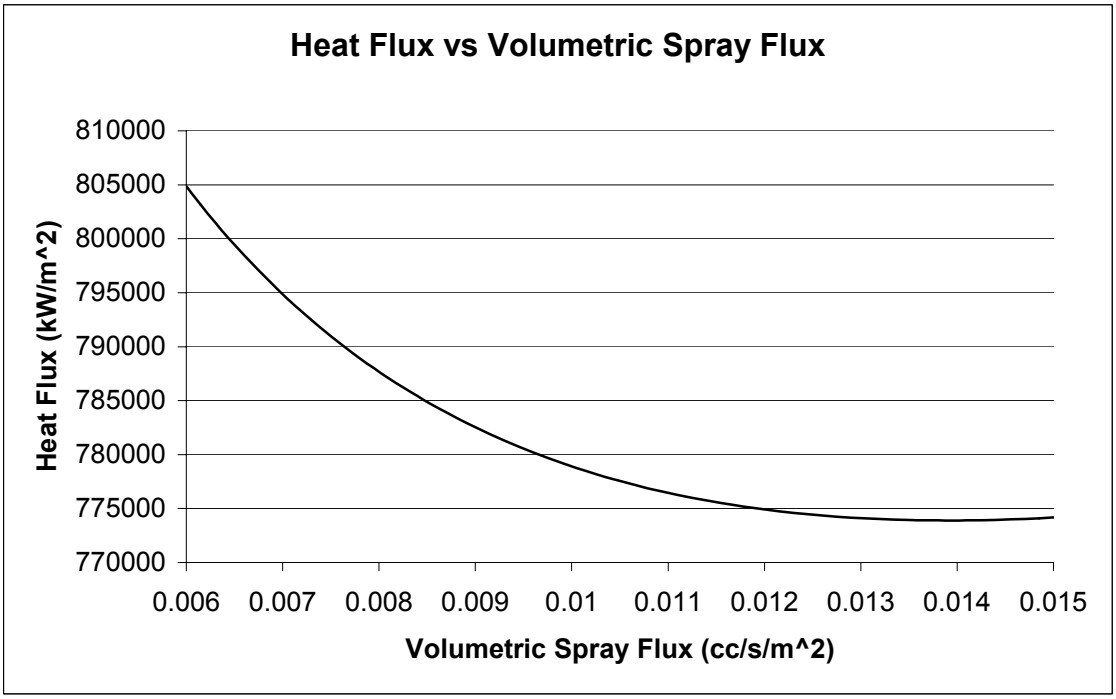


**Figure 3: Heat flux vs Volumetric flux for constant particle diameter and particle velocity.**

These data based on Liu et al [2].

Research by Schmidt, J. and Boye, H. [5] further examined the effect of droplet diameter and velocity on the heat transfer. The purpose of this experiment was to fix the velocity, the volume flux, and vary the droplet diameter to measure the influence of the droplet diameter and the volume flux on the heat flux. The droplet diameter and volume flux were then fixed, and the droplet velocity was varied to test the influence of the droplet velocity on the heat flux. Their results indicated that as the droplet velocity increases, the heat transfer coefficient increases, for the surface temperature interval of $300^{o}$ C ($572\ ^{o}$ F) and $600^{o}$ C ($1112\ ^{o}$ F). For temperatures below this range, the droplet velocity does not affect the heat transfer coefficient appreciably. Contrastingly, in the range of 30 to 110 μm, the heat transfer coefficient is not affected by the droplet diameter. This observation could be attributed to the fact that the surface temperature range is higher for this study than the Liu et al paper.

A study by Pasandideh, M. et al [6] involves a similar experiment to determine the relationship between droplet diameter, velocity and a heat transfer coefficient. In their experiments, they tested a surface temperature range of $50^{o}$ C ($122^{o}$ F) and $150^{o}$ C ($302^{o}$ F) and found that the velocity of the droplets does not affect the heat transfer considerably. Additionally, when the Weber number increases, corresponding to a decrease in temperature, the cooling effectiveness of the spray is independent of the size and velocity of the droplets within the spray. Although it appears that Pasandideh's research contradicts that of Schmidt and Boye, it is important to note that their temperature range is quite different, meaning that Pasandideh was in a different boiling regime, which most likely accounts for the difference.

Tartarini, et al. [7] studied drop wise evaporation and boiling focusing on the behavior of the droplets on solid non-porous surfaces. Their research found that the maximum cooling effect was observed at the middle of a spray. For instance, if there were six droplets, five equally spaced around a center droplet, the center droplet would cool more than the ones around the center droplet. However, if droplets evaporate from the surface too fast, the solid surface would reheat due to the material below the surface. This re-heating would negate the cooling effects of the droplet.

Thomas, R. et al [8] used a finite difference approach and verified the results of Tartarini et al. using experimental values. First, a parameter chi ($\chi$) was defined as the ratio of the airflow rate to the water flow rate. Chi values ranging from 0 to 11.5 were tested on a test piece surface temperature of 1273 Fahrenheit. The nozzle was positioned 0.41 meters above the test piece and the spray area was 10 cm in diameter. The temperatures were recorded and a heat transfer coefficient was estimated. This heat transfer coefficient was then used in a finite element package to predict the thermal stresses, and then the results were confirmed using a finite difference approach. The project team made several important conclusions. An air/water atomizer can be used to adjust the cooling rate from a forging to obtain desired properties without post heat treatment. Second, finite element modeling can reasonably predict temperature distributions within steel. Lastly, a plot of the maximum induced stress versus the temperature at which it occurs can accurately predict the occurrence of cracks due to quenching and over spraying of forgings.

There has not been much research done on pure water atomizing sprays. A study done by Chen et al [9] explores the effects of the spray parameters (droplet size, velocity, and volumetric spray flux) on the critical heat flux on a surface temperature between 800 and

1000 $^{o}$ F (427 to 537 $^{o}$ C). Results of the testing show that the droplet velocity seems to have the greatest effect on the critical heat flux, followed by the droplet flux and then the Sauter mean diameter. In addition, increasing the velocity increases the critical heat flux when the diameter and droplet flux is kept at one value. Similarly, increasing the droplet flux, while keeping the velocity and Sauter mean diameter steady, increases the critical heat flux, but not as much as the velocity. Finally, regardless of how the droplets were formed (pure water or air atomizing) these trends were evident.

## 1.2. Heat Transfer Regimes

It is important to know what boiling regime is involved during spray cooling to be able to characterize and understand the heat transfer coefficient. The surface of the die, during spray cooling, can undergo four regimes, which are natural convection boiling, nucleate boiling, transition boiling, and film boiling. These boiling regimes occur when the surface temperature of the die is much greater than the saturation temperature of the liquid. In the regimes, the heat transfer is accompanied by vapor bubbles and / or pockets of heated liquid that are carried to the surface by buoyancy. The first regime is natural convection boiling characterized by a low excess temperature ($T_{excess} = T_w - T_{sat} \leq 4^{o}C$). In this regime of heat transfer, the convection currents are similar to that shown in Figure 4, assuming a large horizontal die surface and a shallow liquid pool.

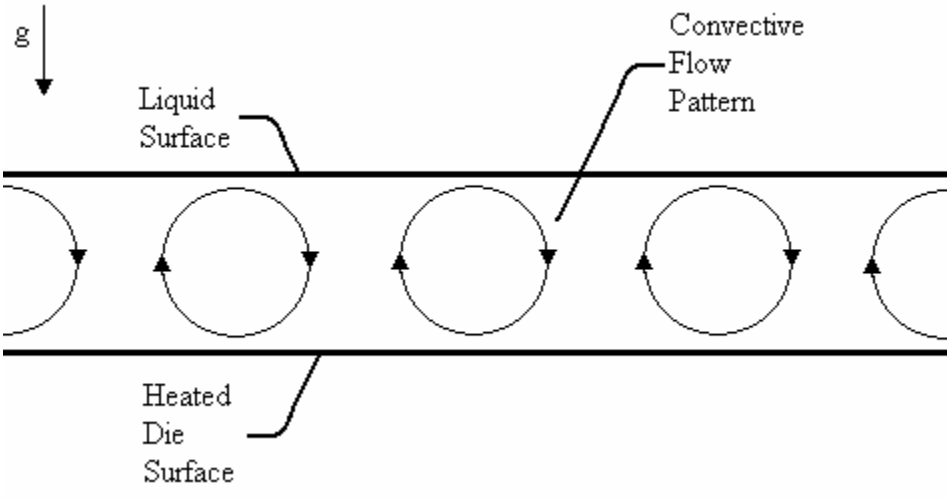


**Figure 4: Convective Currents in Horizontal Fluid Layer [10]**

The next regime is the nucleate boiling characterized by a higher excess temperature. In nucleate boiling, vapor is generated at nucleation sites such as tiny cracks and

imperfections where liquid is trapped and surrounded by large heater area per unit liquid volume. As the excess temperature increases in nucleate boiling, the heat transfer rate increases until the rate peaks at the critical heat flux ($4^{\circ}C \le T_{excess} \le 30^{o}C$). This peak happens at the Leidenfrost point, characterized by even more bubbles increasing in size with higher excess temperatures to the point where the vapor gradually insulates the surface. In this thesis, we concentrate on temperatures above this point. Nucleate boiling has a high heat transfer rate [11]. Just beyond the critical heat flux, the fluid enters transition boiling. Unlike nucleate boiling, the heat transfer rate actually decreases with an increase in excess temperature. The heat transfer rate decreases because the vapor film gradually insulates the surface. The vapor that coats the surface in this regime is unstable, and sometimes is replaced by nucleate boiling. This regime end when the surface is just able to sustain a vapor film at a value called the minimum heat flux ($30^{\circ}C \le T_{excess} = 100^{o} - 200^{o}C$). Finally, past the minimum heat flux, the fluid would enter the film-boiling regime. Here, radiation across the film becomes increasingly important. One can get a better understanding of these regimes by referring to Figure 5. Note that in nucleate boiling, bubbles are replaced by columns and slugs. Transition boiling is a combination of nucleate boiling and film boiling and is not pictured.

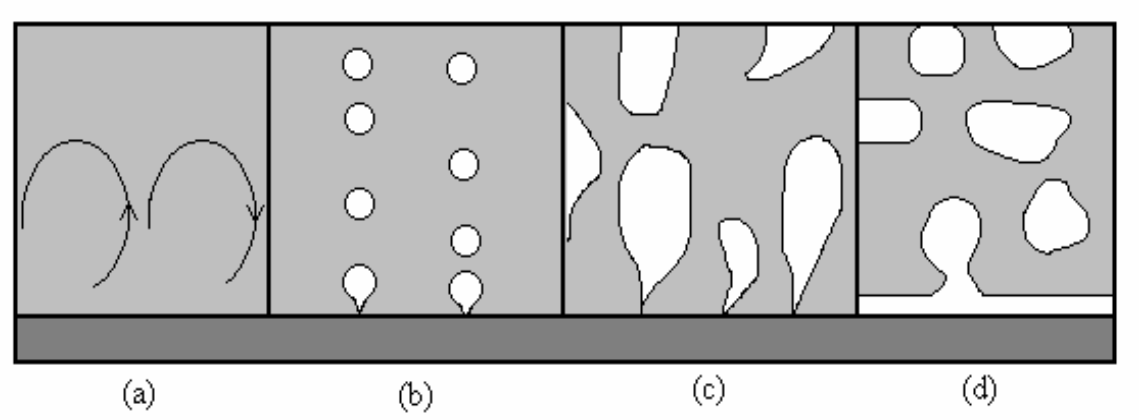


**Figure 5: The four regimes of boiling: (a) Natural convection, (b) isolated bubbles, (c) columns and slugs, (d) film boiling [11].**

## 1.3. Determination of Heat Flux

During the heat conduction experiment (cooling), the temperature of each thermocouple is recorded every second by the LabVIEW software and output to Excel for the test period. To calculate the heat flux for each experiment, a plot must be made in Excel for temperature versus the vertical direction (z) and versus the radial direction (r), then curve fitting the temperature profile. The corresponding temperature profile is then used in equation 6 to find the internal energy (U). Finally using the relationship in equation 7, the average heat flux can be determined by dividing by the surface area. These calculations are repeated at regular time intervals over the entire test period. The advantage to using these relationships is that it provides a simple means to compare test results to other studies. There are a few disadvantages however. In order to get an accurate temperature profile (within 15%), numerous thermocouples are needed to record the temperature gradient.

$$U = \iint \rho 2\pi C_p \, r T(r,z) \, dr \, dz \tag{6}$$

$$-\frac{dU}{dt} = \bar{q} A \tag{7}$$

## 1.4. Determination of Thermal Stresses

The determination of thermal stress is relatively easy if the temperature gradient is known as a function of the distance from the surface and of the radius. Assuming two-dimensional transient temperature, uniform steel properties, unrestrained at the circumference, the instantaneous radial and axial thermal stresses can be determined equations 8 through 10 [13]. There would be thermal stresses in the theta direction, but our assumption is that the temperature gradients are axisymmetric so the circumferential thermal stresses have not been considered. This assumption is justified because the water sprays are designed so that the Sauter mean diameter, velocity and volumetric spray flux are the same circumferentially. In equations 8 through 10, the temperature is a function of the radius r and the vertical distance z, but only integrated over the r direction only.

$$f_r = \frac{-\frac{E\alpha}{r^2}\int_0^r r\,T(r,z)\,dr}{1-\nu} \tag{8}$$

$$f_z = \frac{2N - \alpha E T(r,z)}{1-\nu} \tag{9}$$

$$N = \frac{E\alpha}{r^2}\int_0^r r\,T(r,z)\,dr \tag{10}$$

## 2.0. Sensitivity and Error Analysis

By using a simple error analysis, one can determine the sensitivity of the uncertainty to individual terms in an equation. Equation 11 shows the simplified version of the equation summed over all terms of the stress equation.

$$\delta f = \left[ \left( \frac{\partial f}{\partial E} \delta E \right)^2 + \left( \frac{\partial f}{\partial \alpha} \delta \alpha \right)^2 + \left( \frac{\partial f}{\partial \nu} \delta \nu \right)^2 + \left( \frac{\partial f}{\partial r} \delta r \right)^2 + \left( \frac{\partial f}{\partial T} \delta T \right)^2 \right]^{1/2} \tag{11}$$

The deviations for properties of the material, α, E, and υ, were provided by Finkl, the manufacturer of the steel die. The deviation for r was based upon the accuracy of the measuring instrument. Examining each term individually, one can determine the relative contribution of each term to the overall uncertainty. Computing the partial derivatives and substituting in the values for the parameters and the deviations can be done in any popular equation solving software such as MathCAD, Maple, or MatLab. The results are summarized in the following table.

The error for the temperature profile is from two different sources. First, there is an error from the thermocouples. The temperature can only be collected within an accuracy of 6 percent above and below the recorded temperature due to the thermocouple inaccuracy. The other source of error for the temperature profile is within the curve fit of the profile based on the number of thermocouples that are recording the temperature. Obviously many thermocouples would create a more realistic profile than two thermocouples. Based upon an analysis of a comparison of the curve fit of a profile created by thermocouples and the actual calculated profile, four thermocouples were chosen as an accurate representation of the curve. The difference in the $R^2$ value between four thermocouples and six or eight was only

about 6.5 percent; this is not cost effective to make it worth buying the extra expensive thermocouples.

| Parameter (X) | δX | $\frac{\partial f}{\partial X}$ | $\left(\frac{\partial f}{\partial X}\delta X\right)^2$ | Percent Contribution to total error | Error |
|---|---|---|---|---|---|
| α | 1E-6 m^2/s | 0.715E15 | 0.51E26 | 11.91 | |
| E | +/- 10 GPa | 0.03 | 0.892E18 | 1.412 | |
| T | +/-258.15 deg K | 0.255E7 | 0.434E17 | 0.393 | |
| υ | +/- 0.01 | 0.8824E10 | 0.779E16 | 0.485 | |
| r | +/- 0.01 m | 0.306E7 | 0.234E11 | 0.131 | |
| Total | ——— | ——— | 0.51E26 | 13.09 | +/-1.43 E11 Pascal |

**Table 1: Sensitivity Analysis**

In this table, the individual terms of equation 11 are broken down. The percent contribution column breaks down the contributions of each parameter to the total error of 13.1 percent. The total is the deviation of the thermal stress (δf) is listed in the last column. Now one can go back, look at this table, and determine what variables can be determined more accurately to reduce the overall uncertainty. In addition, if there is a large change in a metal property, one can view this table and determine if it would have a huge impact. For example, if there were a large variation in the thermal conductivity (α) then the uncertainty would be affected much more than if inaccurate thermocouples were used for temperature measurement.

# 3.0. Experimental Methods and Procedure

For this thesis, a laser PDA system was used to determine the flow parameters of Sauter Mean Diameter, average droplet velocity, and volumetric spray flux from both water and air atomizing nozzles. Five types of nozzles were tested, four water driven, one air-atomizing nozzle. To determine the thermal stresses and heat flux, a heat conduction experiment using a test piece and the tested nozzles was performed at Wyman-Gordon's Research and Development division.

## 3.1. Spray system

The atomizing system, used for both the air atomizing and the pure water atomizing tests, was constructed as pictured in Figure 6. The spray nozzles at the bottom of the system were supplied by Spraying Systems Co. They include the models 1/4J+SV11, 1/4G 6.5, 1/4G 12.5, and 3/4HH-SS 50SQ. For the water-atomizing nozzle, the water pressure was assisted by air pressure to increase the water pressure (note compressed air was not used to atomize the particles, just to increase the pressure of the water). For the air-atomizing nozzle, a valve leading to the water tank was closed and another valve was opened. Now, the air, instead of being used to pressurize the water, is separate from the water line so the two lines can now be fed to the air-atomizing nozzle. The pressure gage for both lines for the air-atomizing nozzle was at the end of the line. Additionally, the pressure gage for the water-atomizing nozzle was located upstream of the actual nozzle, allowing for pipe losses. A flow meter was also connected to the line to verify the flow rate. The distance to the sample is another variable of concern. Due to the sensitivity of the PDA system, to record closer than 36 inches makes the system very inaccurate and impractical to run the measurements.

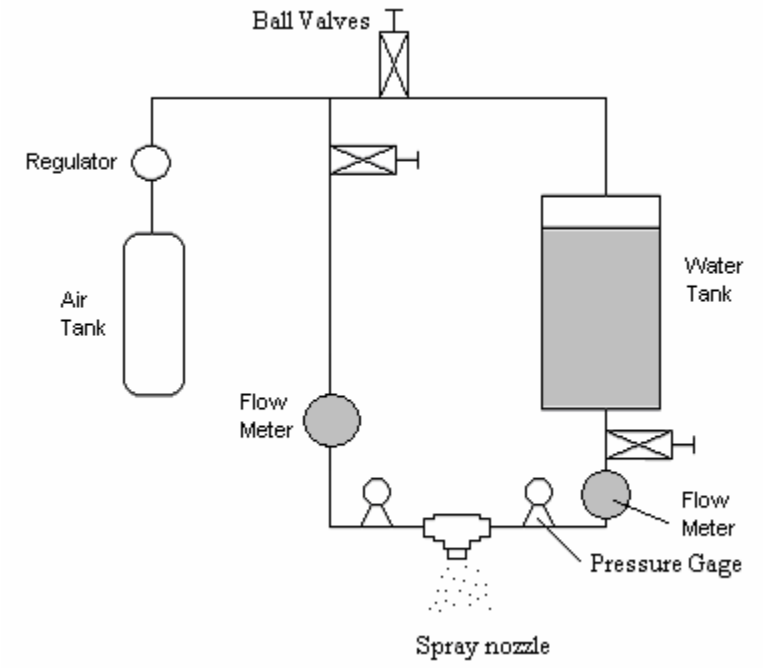


**Figure 6: Schematic of Spray Setup**

## 3.2. PDA System

In order to measure particle Sauter Mean Diameter, average velocity, and volumetric spray flux, a Dantec Particle Dynamic Analyzer system was used. The analyzers consist of a transmitter, receiver, a signal processor, and a computer shown in Figure 7.

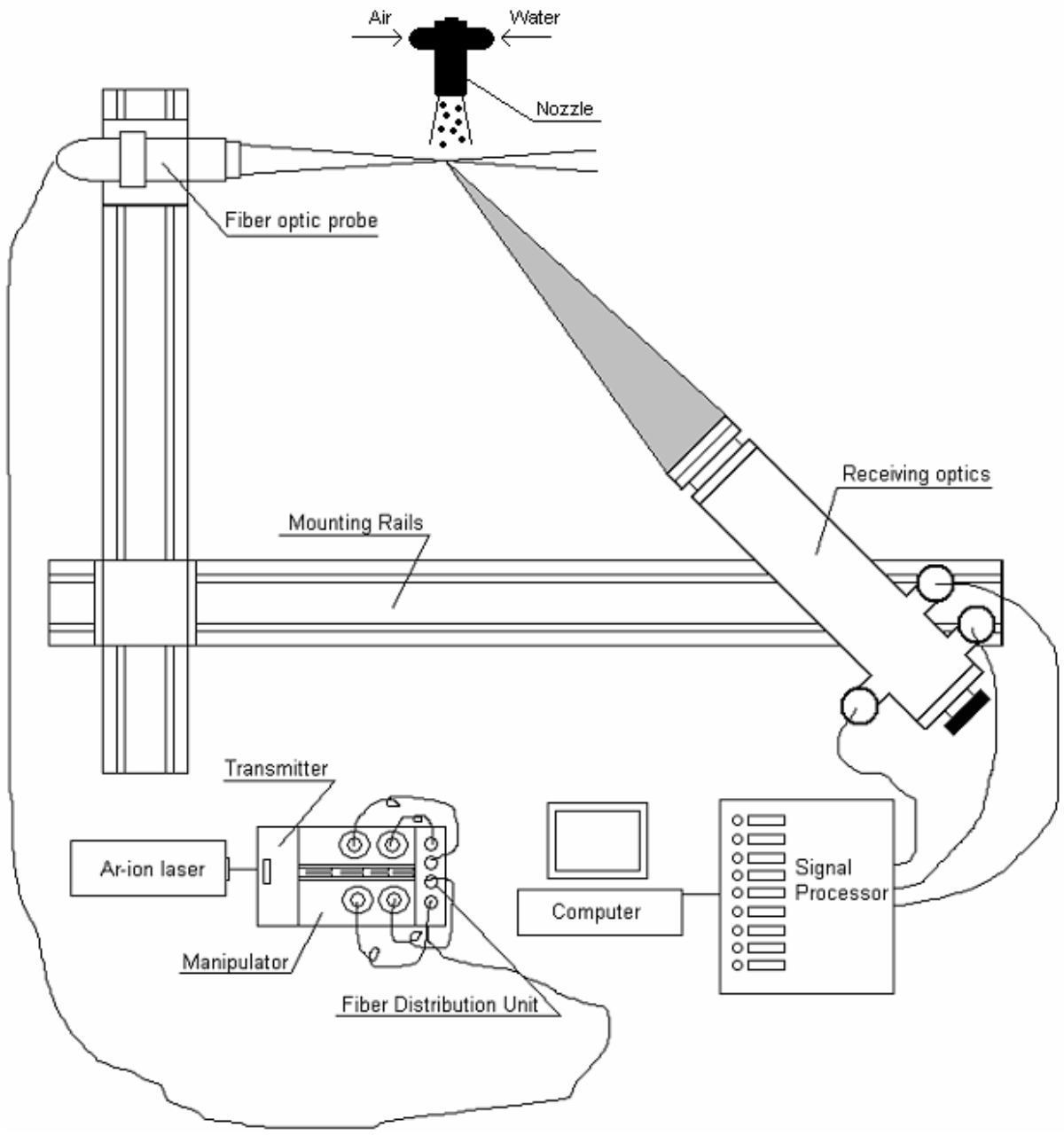


**Figure 7: PDA setup**

The interrogation volume is bound by the intersection of the transmitting laser beam and the receiving optics range of focus. When a drop passes through this site the light is scattered forming an interference fringe pattern. The interference pattern detected by the receiver is

related to the Doppler frequency shift, which in turn is proportional to the drop velocity. The spatial variation in the fringe pattern is proportional to the droplet diameter. On the transmitter, a beam splitter, Brag cell, beam spacer, and a fiber optic module with a 150-mm focal length were used. For the receiving optics, the frequency shift was set to 10 MHz for the smaller diameters and velocities, 100 MHz for the larger diameters and velocities expected. Using these results, measurements are accurate to within 6 percent of the actual Sauter mean diameters, particle velocities, and volumetric spray flux.

To obtain the spray characteristics, the nozzle was connected to the piping system and, since the piping system was connected to a moveable stand, the height (most were done at 3 feet from nozzle to sample volume) and distance from the center (between 0 and 3 inches) of the spray was set by moving the stand into the correct position. The pressure to the nozzle was then adjusted, in the range of 30 psi to 150 psi, and then increased until the desired test pressure at the nozzle was reached. At this point, the PDA laser was turned on, and the software SizeWare was run. Data points were collected every 0.5 seconds for 30 seconds or 5000 samples which ever came first. Then the data, consisting of the Sauter mean diameter, average velocity, and volumetric spray flux, were recorded by the software and entered into Excel for analysis after the experiments had been run. Two tests were run for each of the nozzles, both for the flow parameter variation from the center and over the different pressures, and the results were averaged and double-checked for anomalies.

## 3.2. Heat Conduction Experiment

For the heat conduction experiment, an induction coil was used around a 16-inch circular steel test piece to heat the entire sample. Thermocouples were positioned as pictured in Figure 8. They were positioned as such to allow examination of penetration temperature gradients as well as radial temperature gradients. The test piece was heated up to around 1000 degrees Fahrenheit throughout the test piece. The spray was then adjusted to cover only 10 inches of the full 14 inches in order to obtain a temperature profile in the radial direction. Then, the surface was cooled to an operating temperature of 540° Fahrenheit, a temperature supplied by Wyman-Gordon based upon their research. Temperatures were recorded every half a second and the temperature profile was calculated using a best-fit trend line in Excel. The axial and radial temperature profiles were then used to predict the thermal stresses.

| T/C # | Depth | Location from edge |
|---|---|---|
| 1 | 1 | 7 |
| 2 | 2 | 7 |
| 3 | 4 | 7 |
| 4 | 1 | 4.5 |
| 5 | 1 | 2 |
| 6 | 1 | 0.75 |
| 7 | 2 | 4.5 |
| 8 | 2 | 2 |
| 9 | 2 | 0.75 |
| 10 | 4 | 4.5 |
| 11 | 4 | 2 |
| 12 | 4 | 0.75 |

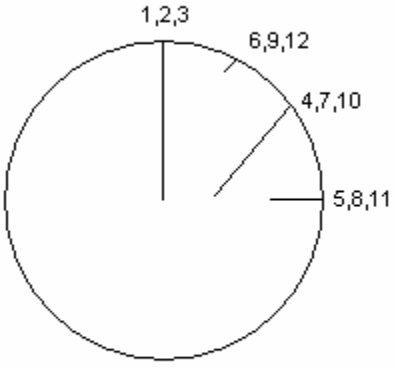


**Figure 8: Thermocouple positions on 14-inch diameter by 8-inch long test piece (depth and location have the units of inches)**

# 4.0. Results and Discussion

## 4.1. Spray Characteristics

The first nozzle is the water driven nozzle model 1/4G 6.5 with a 0.096 inch orifice diameter and circular cone spray pattern from Spraying System Inc. An extensive study was done on this particular nozzle since it is representative of a typical water atomizing nozzle's spray characteristics. Additionally it was to be used in the heat transfer experiment so a detailed analysis would be useful to better understand those results as well. One can see in Figure 9, the diameter varies with position as an inverse gaussian. On the other hand, in Figure 10 the average velocity profile is gaussian. As pressure increases, this trend becomes more evident. Finally, in Figure 11, the volumetric spray flux also decreases with distance but in a more linear trend than the diameter or velocity.

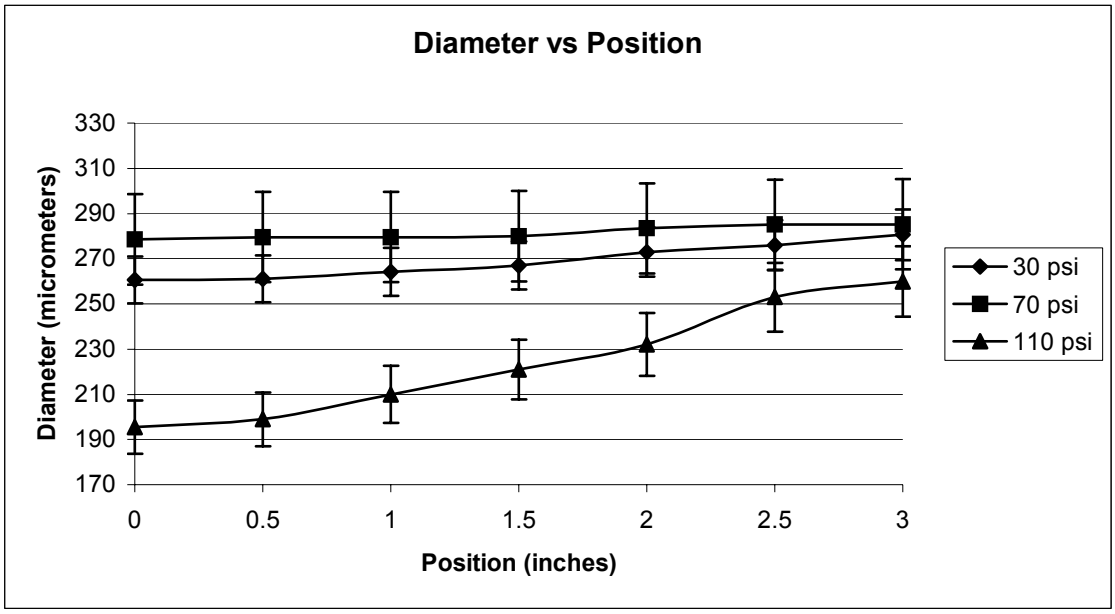


**Figure 9: Particle diameter as measured from the center of the spray**

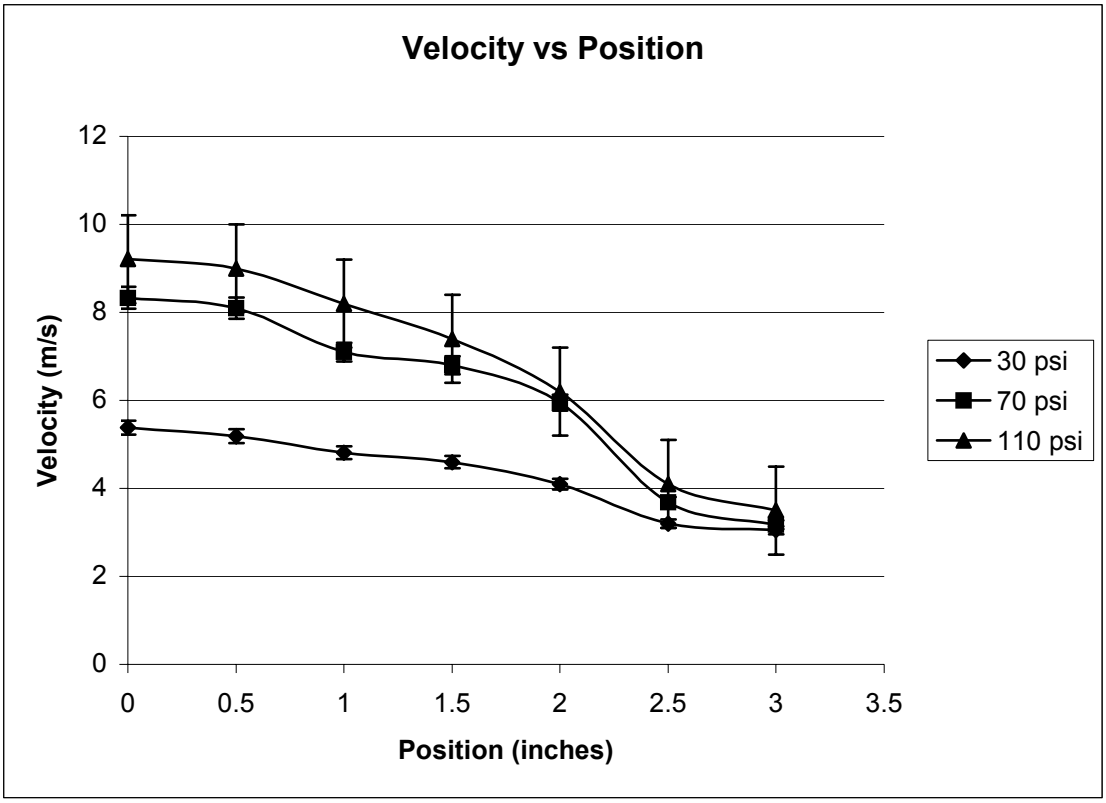


**Figure 10: Volumetric spray flux as a function of distance**

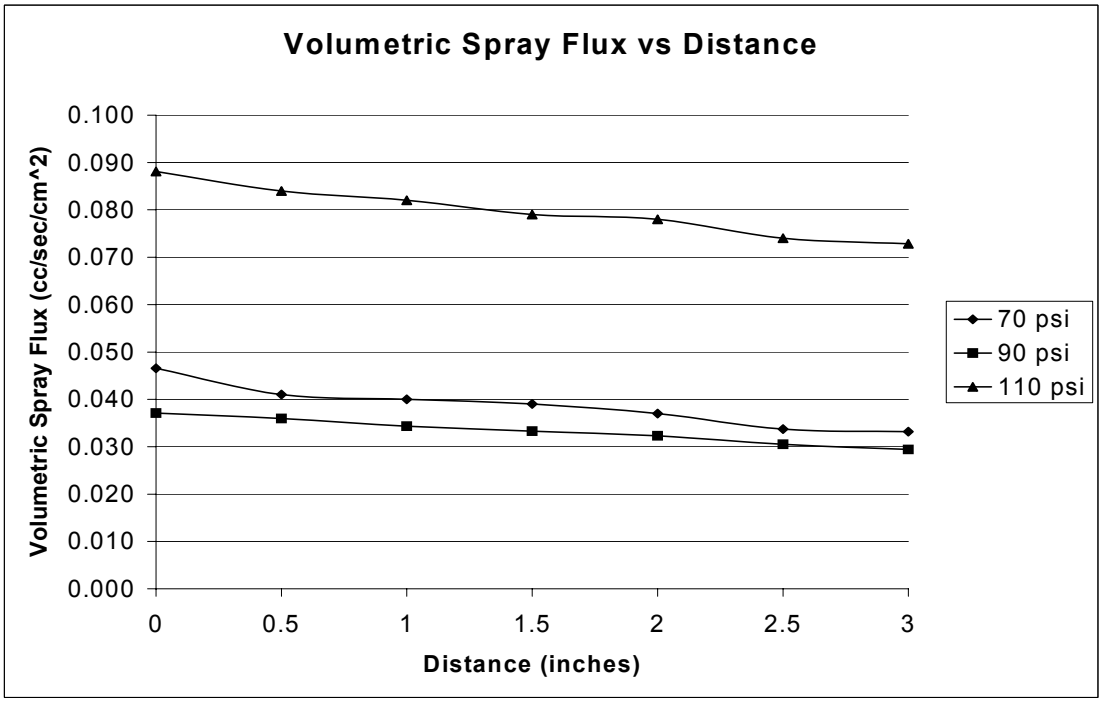


**Figure 11: Particle velocity as measured from the center of the spray**

When one plots the average velocity and volumetric spray flux versus pressure, Figures 12 and 13 respectively, a clear trend of increasing velocity can be observed. This is as one would expect.

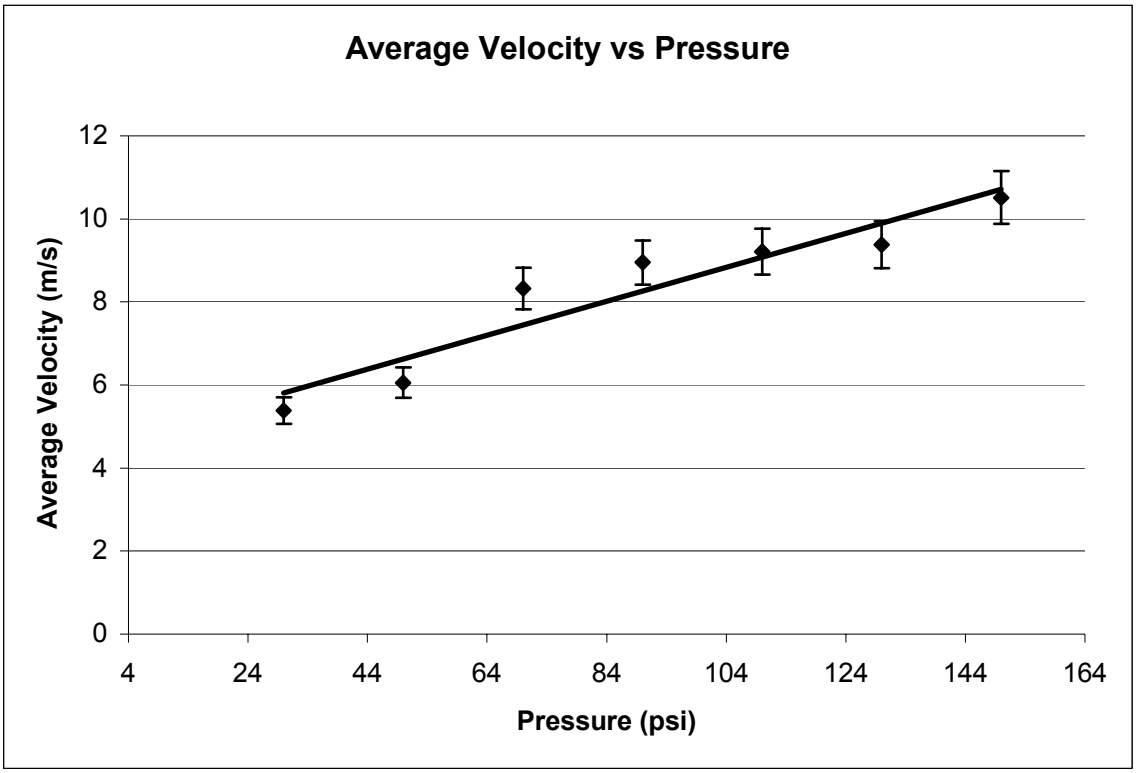


**Figure 12: Smaller orifice average velocity results**

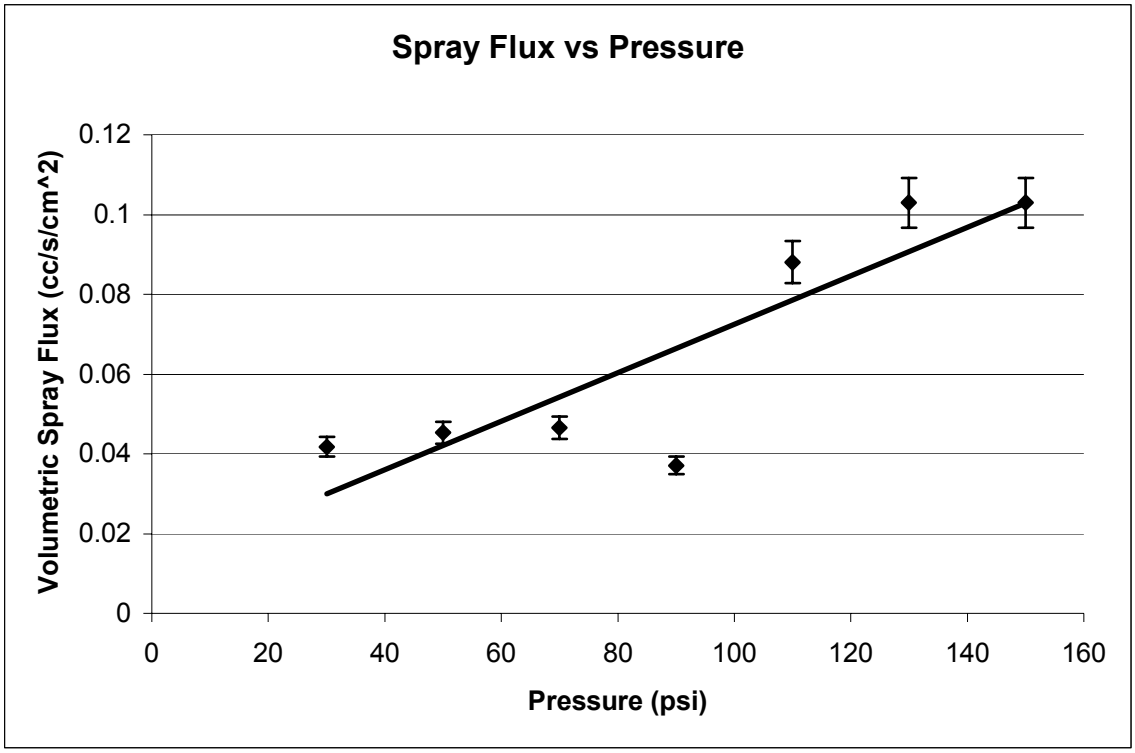


**Figure 13: Smaller orifice volumetric spray flux results**

However, the diameter takes more of a backward "C" curve, shown in Figure 14. At first, this curve may not make sense, but some sort of choking effect may be causing this shape. The data is repeatable since the experiment was run twice and twice this pattern was shown; the values reported are the average between the two tests.

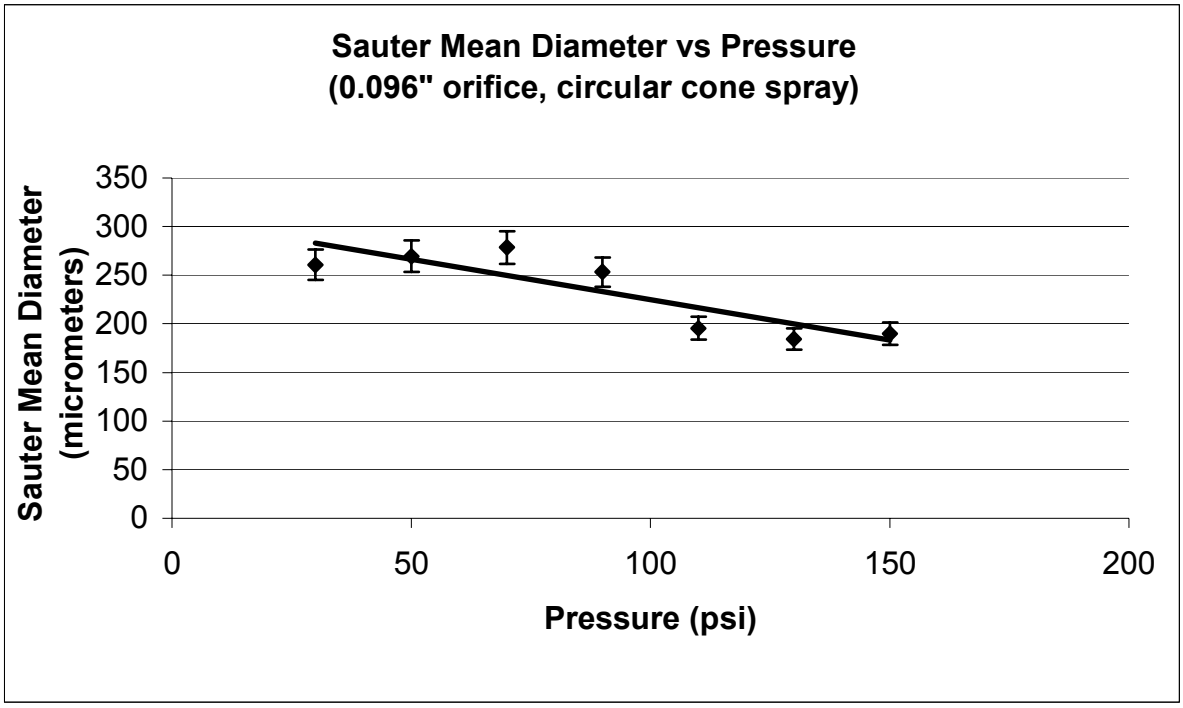


**Figure 14: Sauter mean diameter results for smaller orifice nozzle**

Finally, when the theoretical heat flux is calculated as done in Liu et al [4], and averaged, by distance from center, heat flux is nearly independent of the pressure (shown in Figure 15). The heat flux is distance averaged by multiplying the distance from the center (X) by the heat flux (q) as shown in equation 12.

$$\bar{q} = \frac{\sum Xq}{\sum q} \tag{12}$$

Because the testing done by Liu et al does not use the same testing parameters, their calculations may not be reliable. Too many other factors including the higher temperature of the test piece may affect these results.

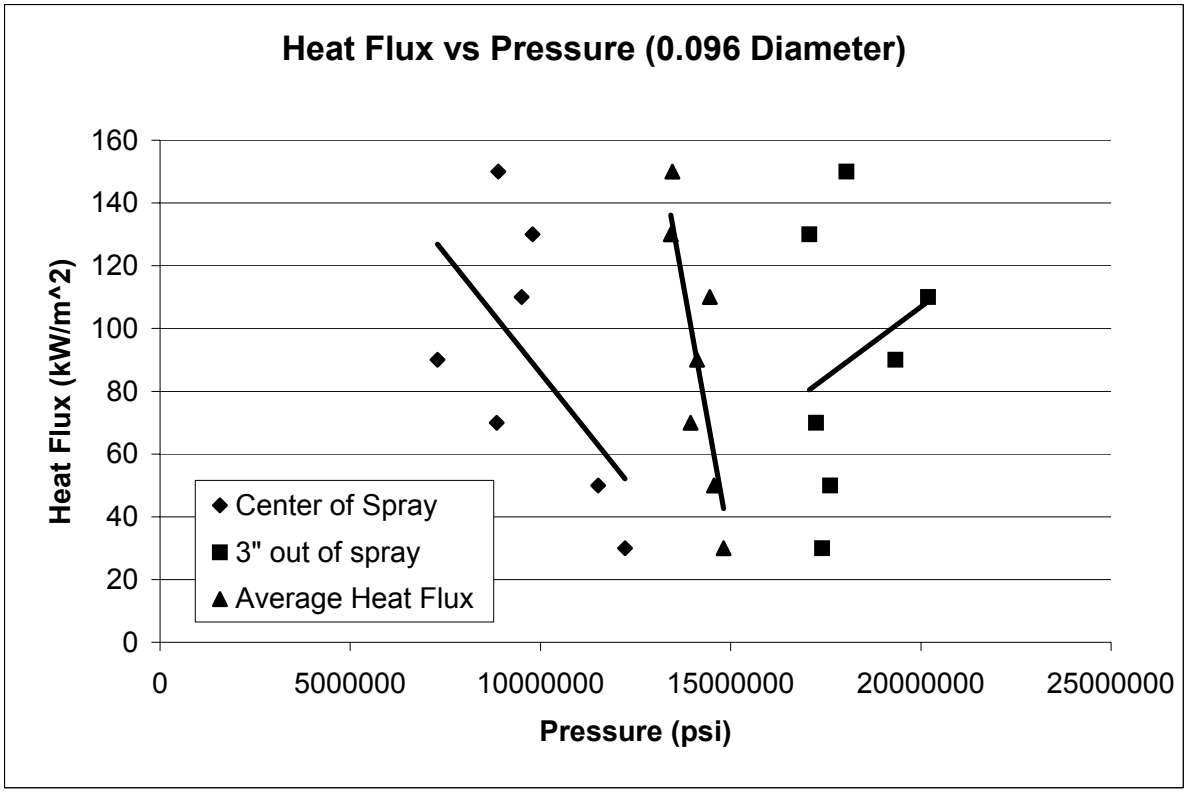


**Figure 15: Approximate heat flux in smaller orifice nozzle**

The larger orifice (0.125 inch) circular cone spray produced results similar to the smaller orifice circular cone spray. The volumetric spray flux, Figure 16, and the average velocity, Figure 17, increase with increasing pressure, which is expected. Additionally, the recorded flow rates in Figure 18 correspond within 10 percent of the values experimentally found by Spraying Systems Inc.

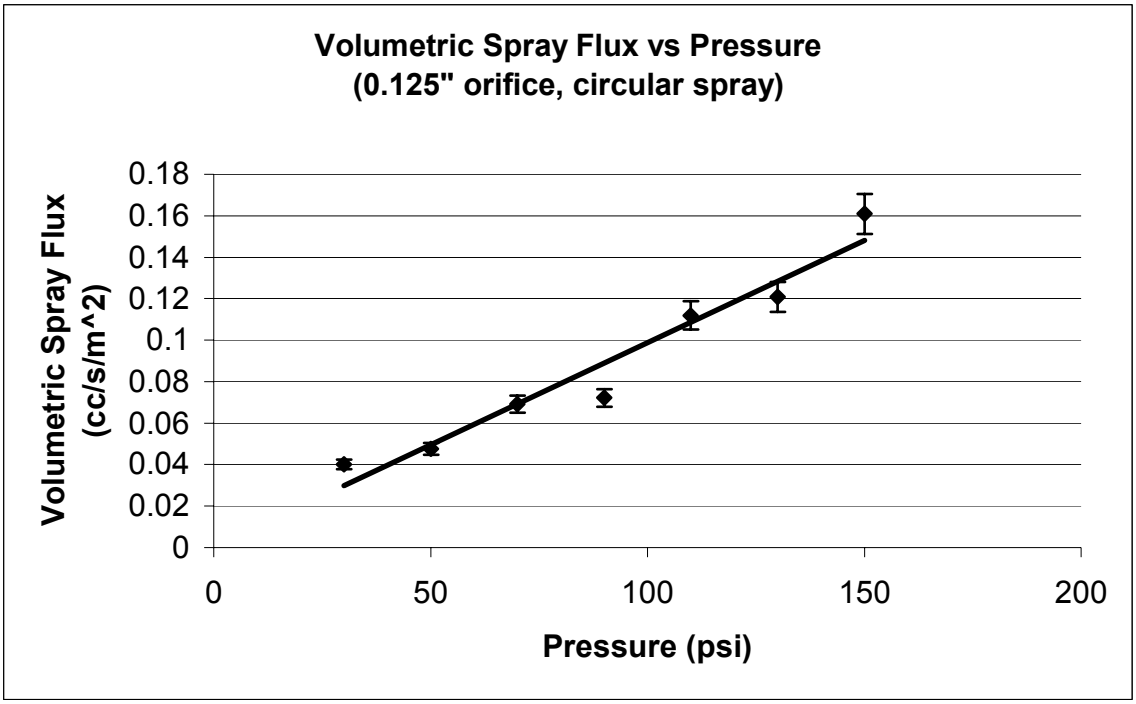


**Figure 16: Volumetric Spray Flux results for larger orifice circular spray**

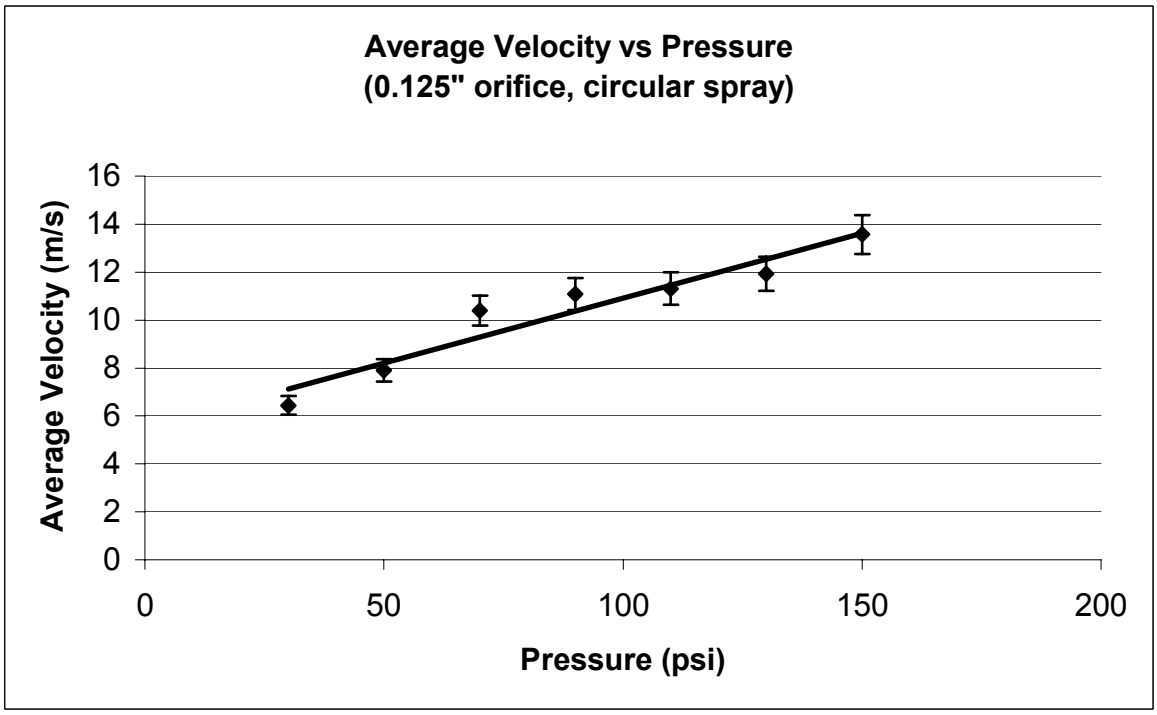


**Figure 17: Average velocity results for larger orifice circular spray**

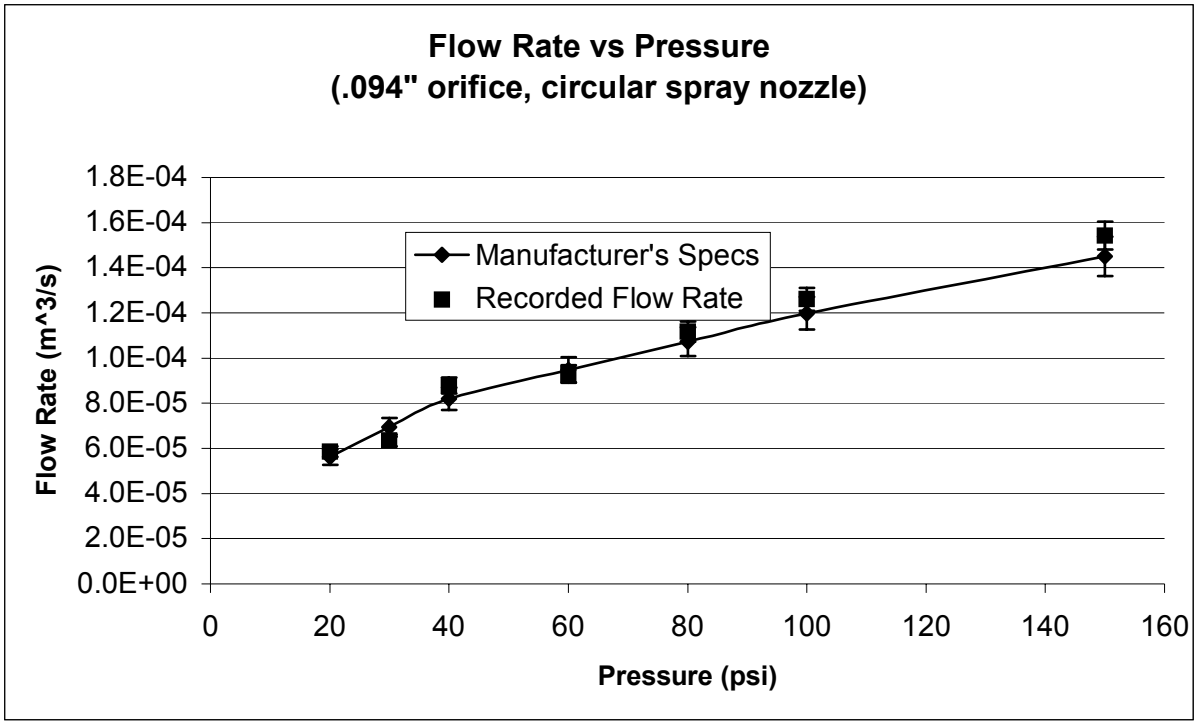


**Figure 18: Manufacturer's flow rates and actual flow rates for smaller orifice nozzle**

Again, the Sauter mean diameter, Figure 19, forms an "C" shape, probably due to some type of choking effect. Although detailed experiments were not done on this nozzle, the theoretical heat transfer, Figure 20, was approximately the same as the smaller orifice nozzle. The Sauter mean diameter, particle velocity, and volumetric spray flux should increase with an increase of the orifice size and such an increase is shown by comparing Figure 21 (0.125" orifice) with Figure 18 (0.096" orifice). Therefore, we can predict that the shape of the velocity and diameter curves from the center should be similar.

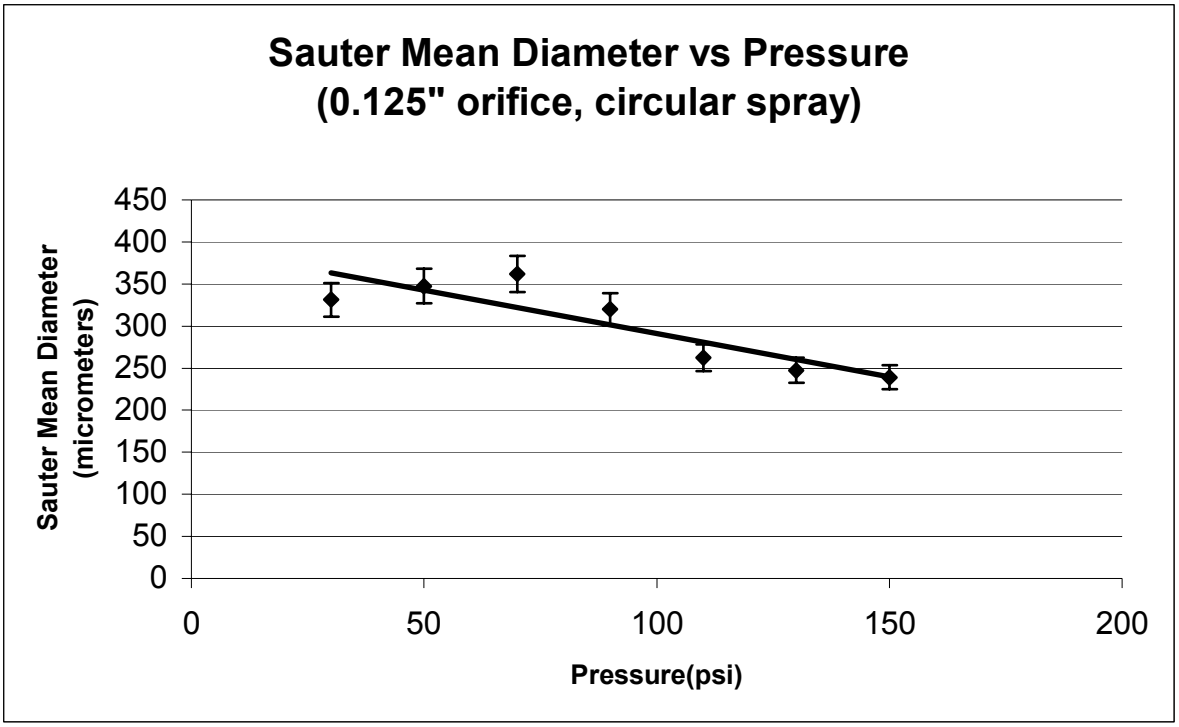


**Figure 19: Sauter mean diameter results for larger orifice circular spray**

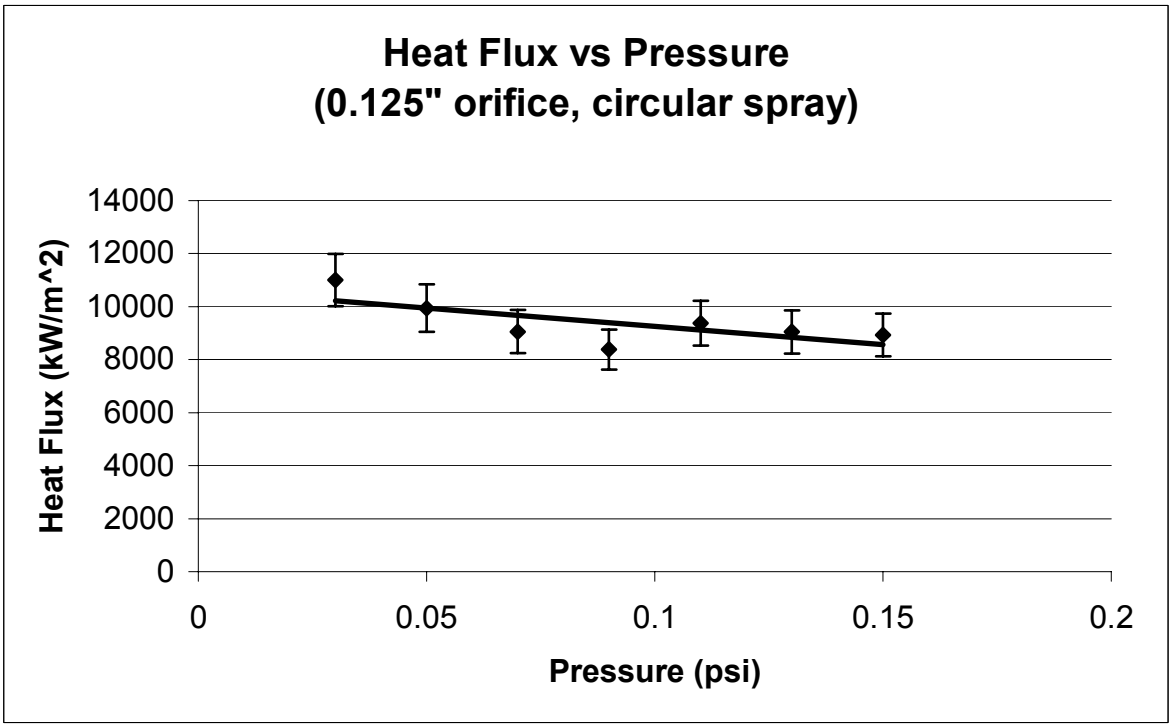


**Figure 20: Estimated heat flux results for larger orifice circular spray**

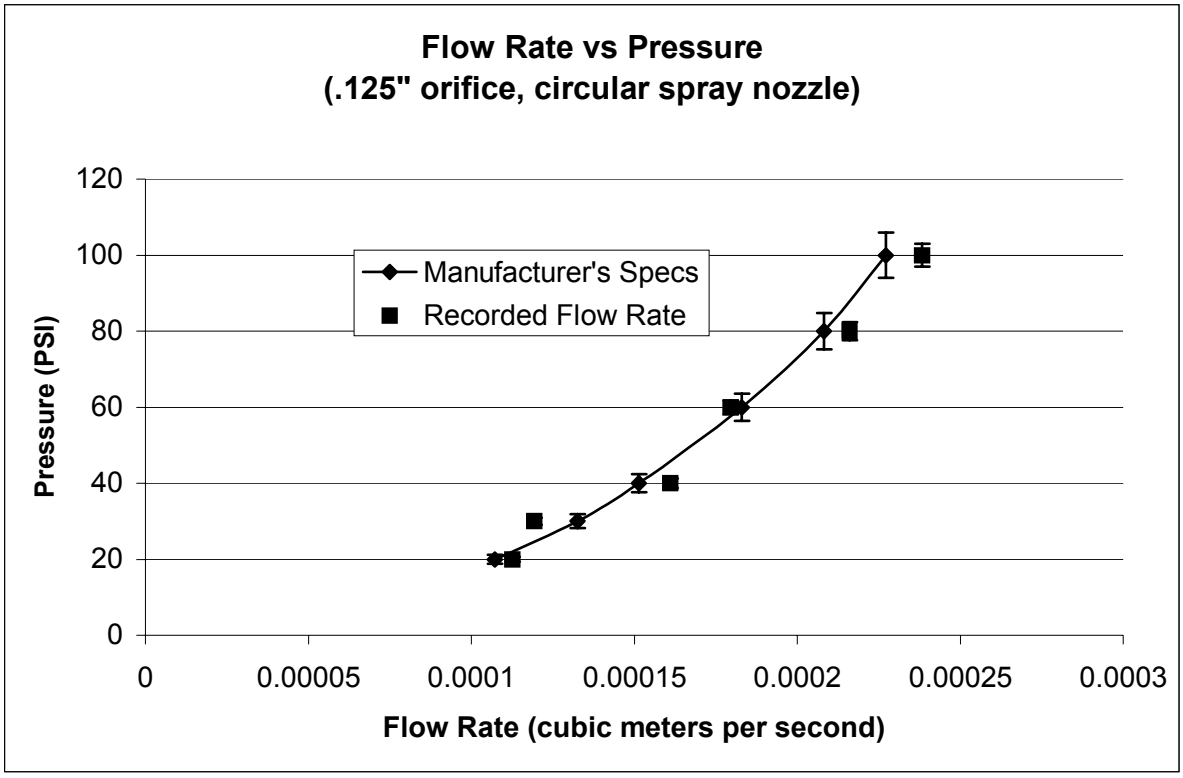


**Figure 21: Manufacturer's and actual flow rates for larger orifice nozzle**

Next, the square spray nozzle was examined. Although the nozzle produces a different shape of spray, again similar trends were observed. The average velocity and volumetric spray flux increase with pressure, as do the other two spray nozzles (Figures 22 and 23).

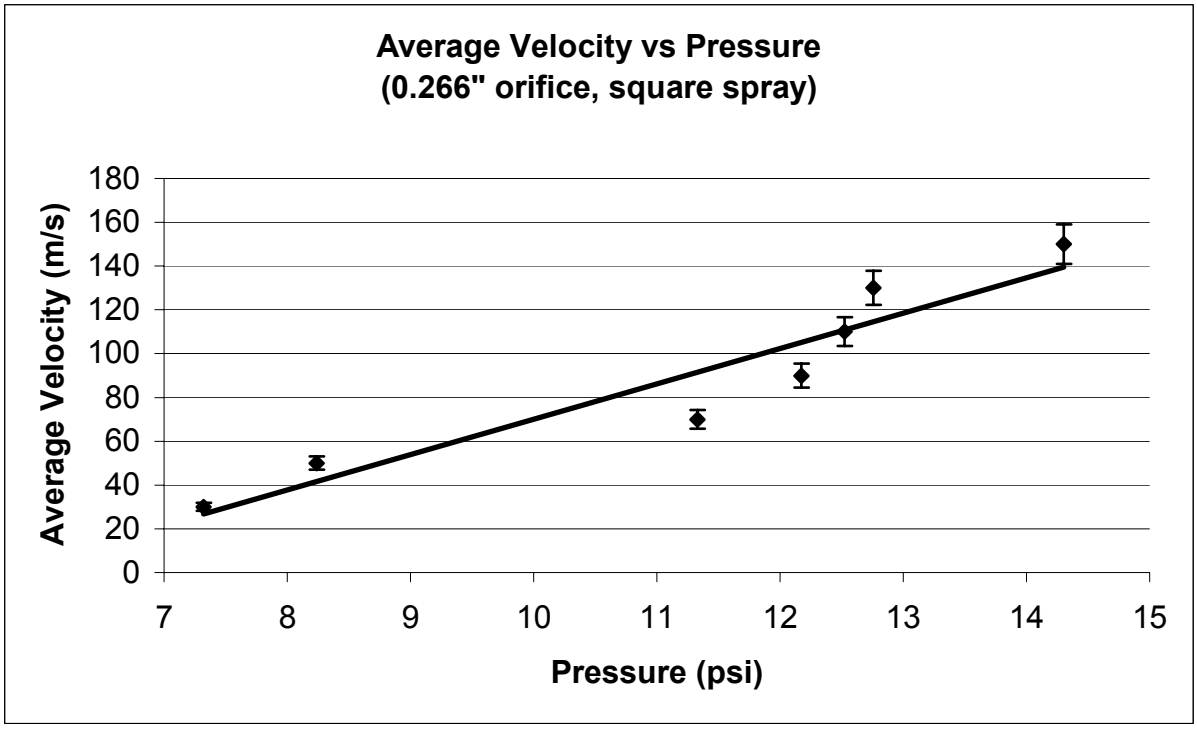


**Figure 22: Average velocity results for square spray**

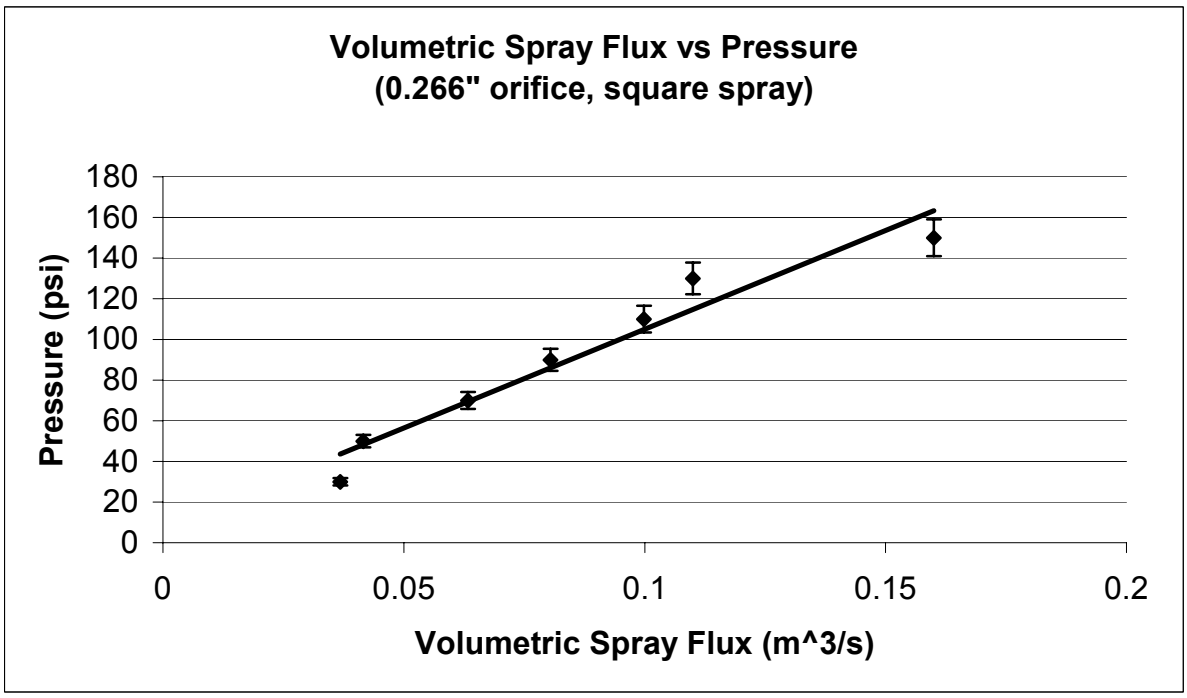


**Figure 23: Volumetric spray flux results for square spray**

The Sauter mean diameter has a decreasing trend as shown in Figure 24. The difference between the conical sprays and the square spray is in the theoretical heat flux (Figure 25). Since the orifice size increases, it makes sense that the Sauter mean diameter and volumetric spray flux increase. However, because the shape of the spray is square instead of conical, the radial variation of the Sauter mean diameter, particle velocity, and volumetric spray flux may be quite different than the 0.096 inch orifice results for the radial variation. Further experimentation may be needed if this nozzle is to be used. Finally, the flow rates are shown in Figure 26, and as with the other two nozzles, the actual and the manufacturer's values are within 10 percent of each other.

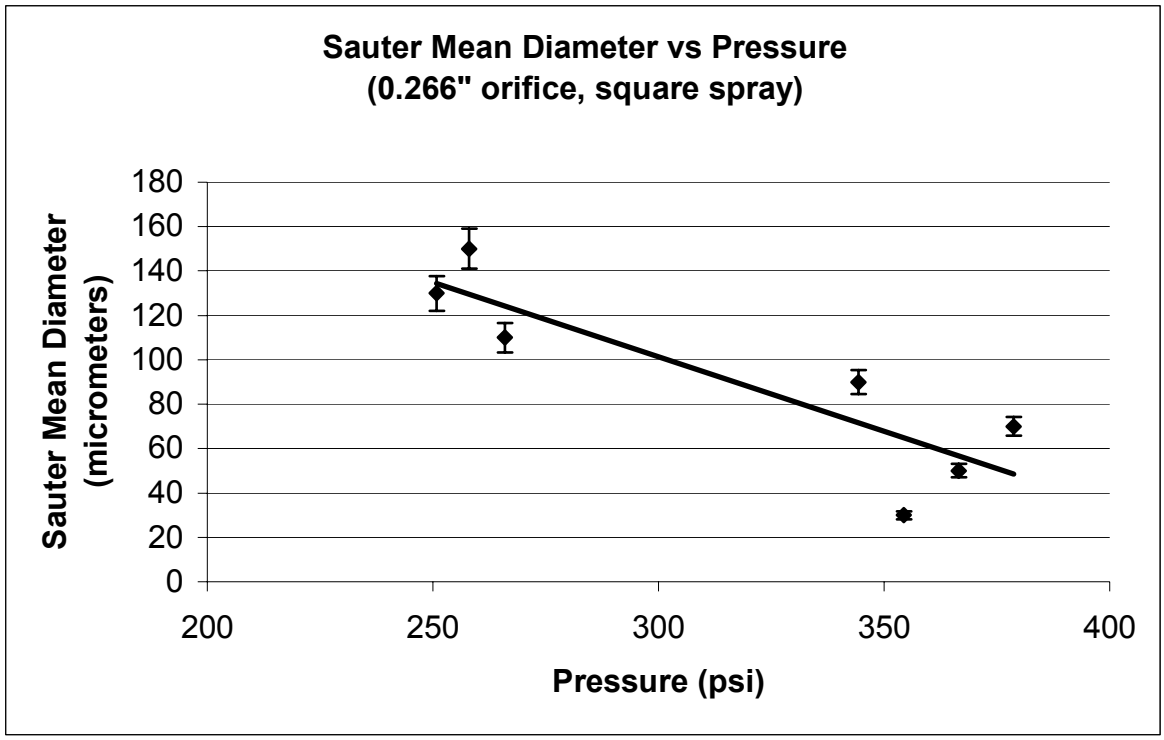


**Figure 24: Sauter mean diameter results for square spray**

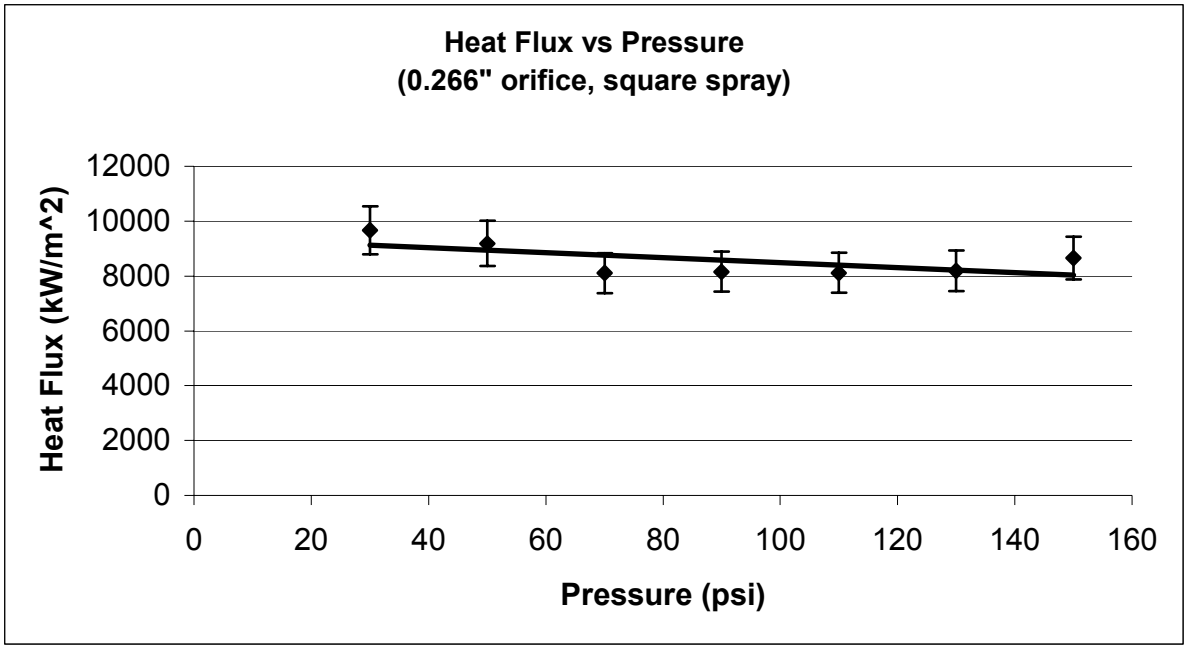


**Figure 25: Estimated heat flux results for square spray**

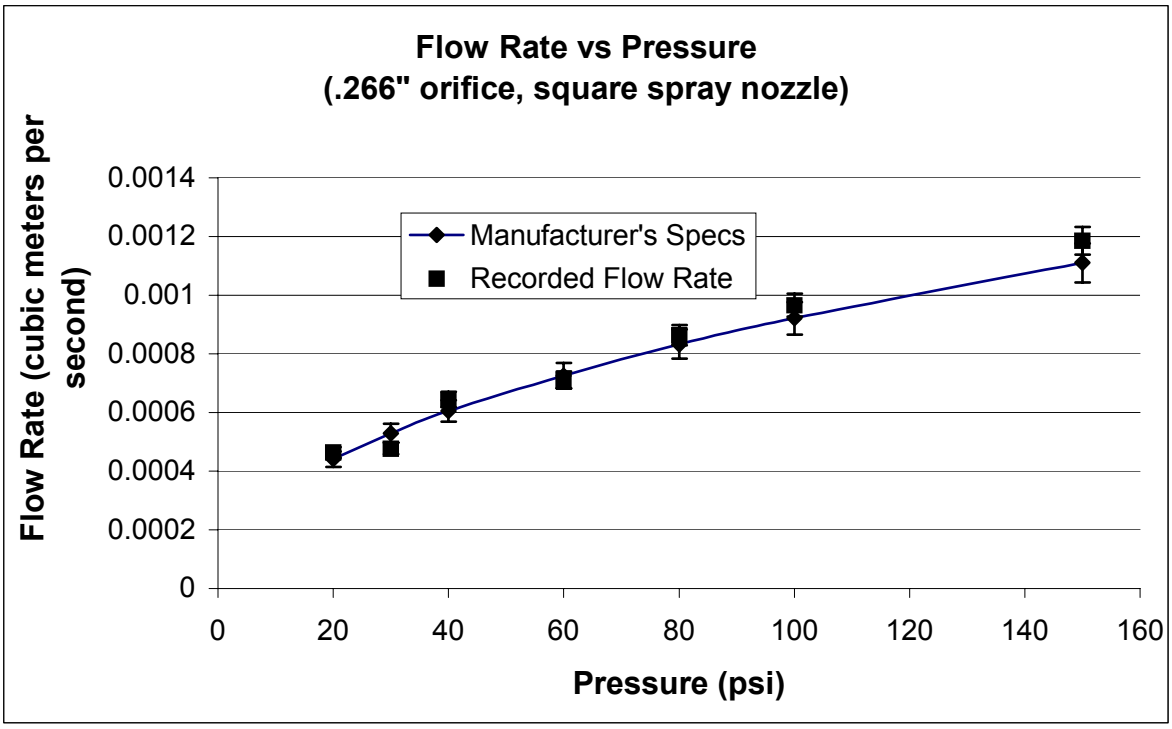


**Figure 26: Manufacturer's and Actual flow rates for the square spray nozzle**

The air-atomizing nozzle is different from the water atomizing nozzles. With this nozzle set-up, smaller and faster droplet sizes could be produced, while the volumetric spray

flux decreased as compared to the previous nozzles. In general, the volumetric spray flux, Figure 27, and the droplet velocities, Figure 28, increased with pressure with some minor variations. As expected, the Sauter mean diameters for the air-atomizing spray are significantly lower than the water atomizing nozzles (Figure 29).

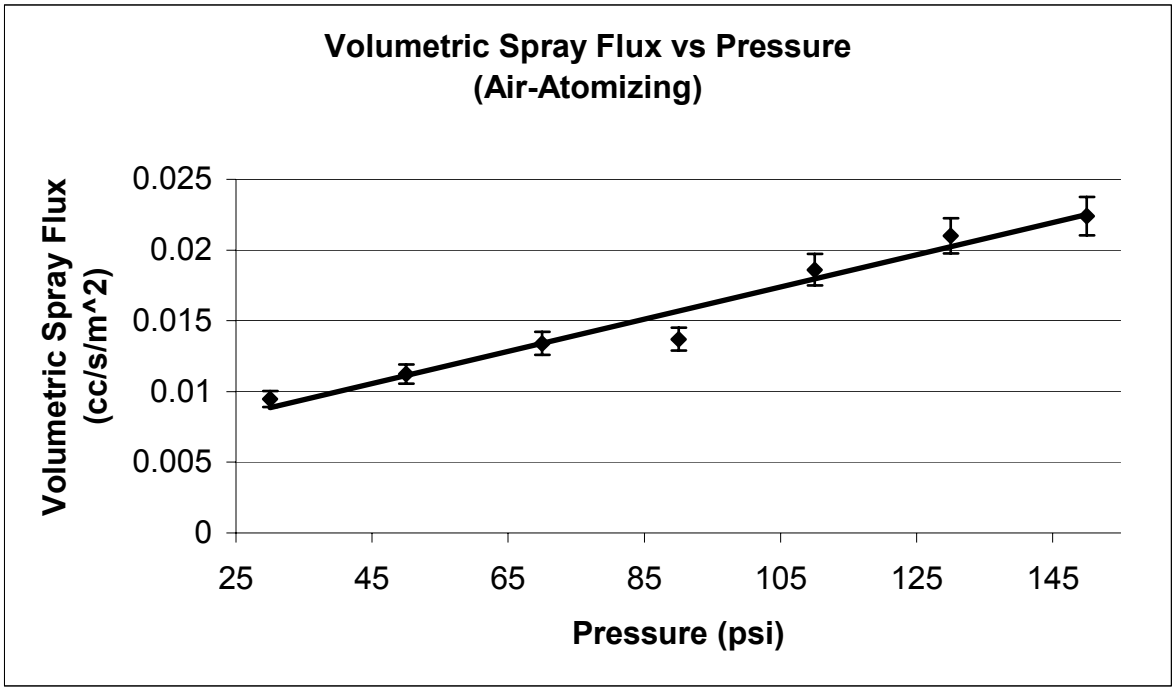


**Figure 27: Volumetric spray flux results for air atomizing nozzle**

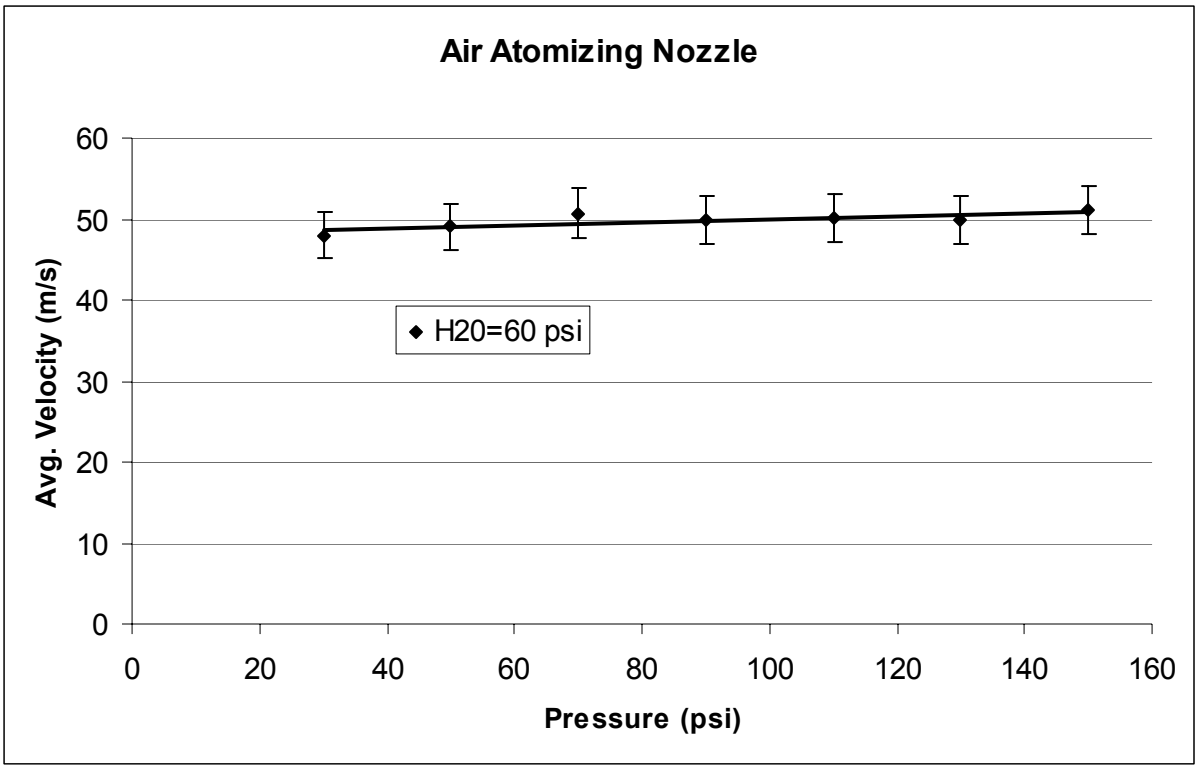


**Figure 28: Average velocity results for air atomizing nozzle**

Figure 30, shows that this decrease in the spray flux translates into a heat flux approximately 30 times smaller than the water driven nozzles. The decrease in the heat flux should lead to lower cooling rates during the heat conduction experiments. The flow rates in Figure 31 are also consistent with what the manufacturer suggests and much lower than those produced by the water nozzles.

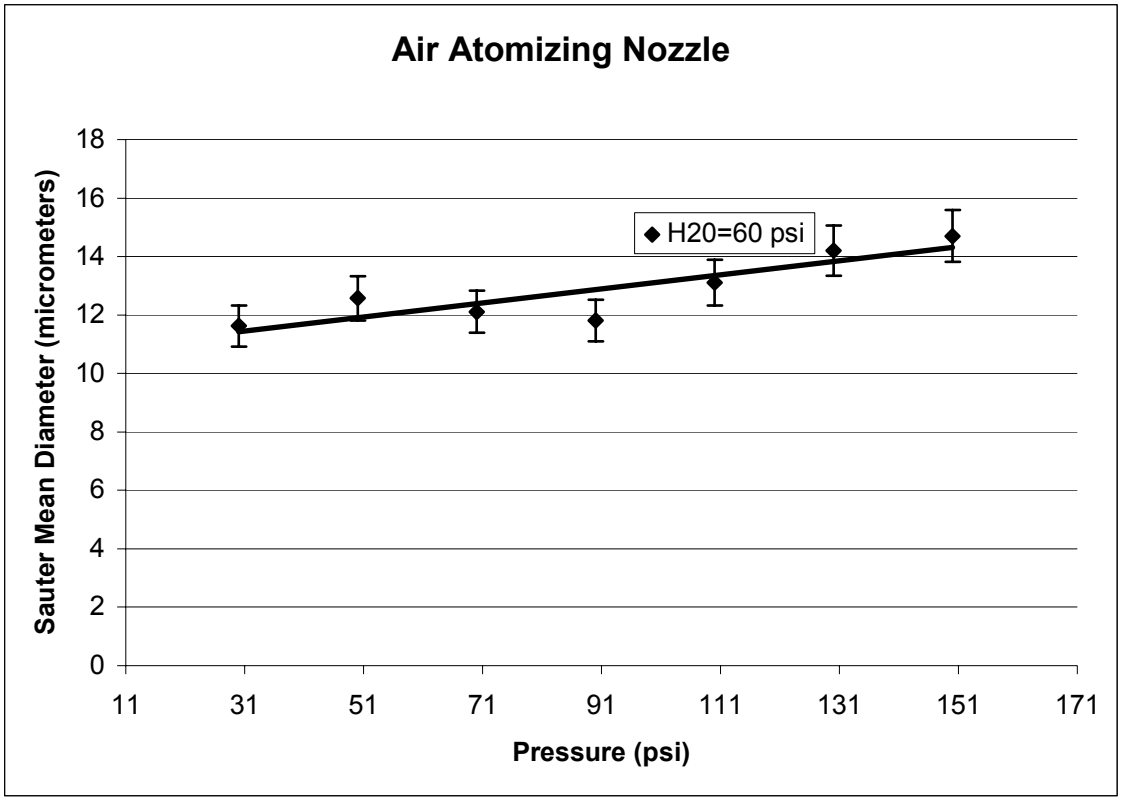


**Figure 29: Sauter mean diameter results for air atomizing nozzle**

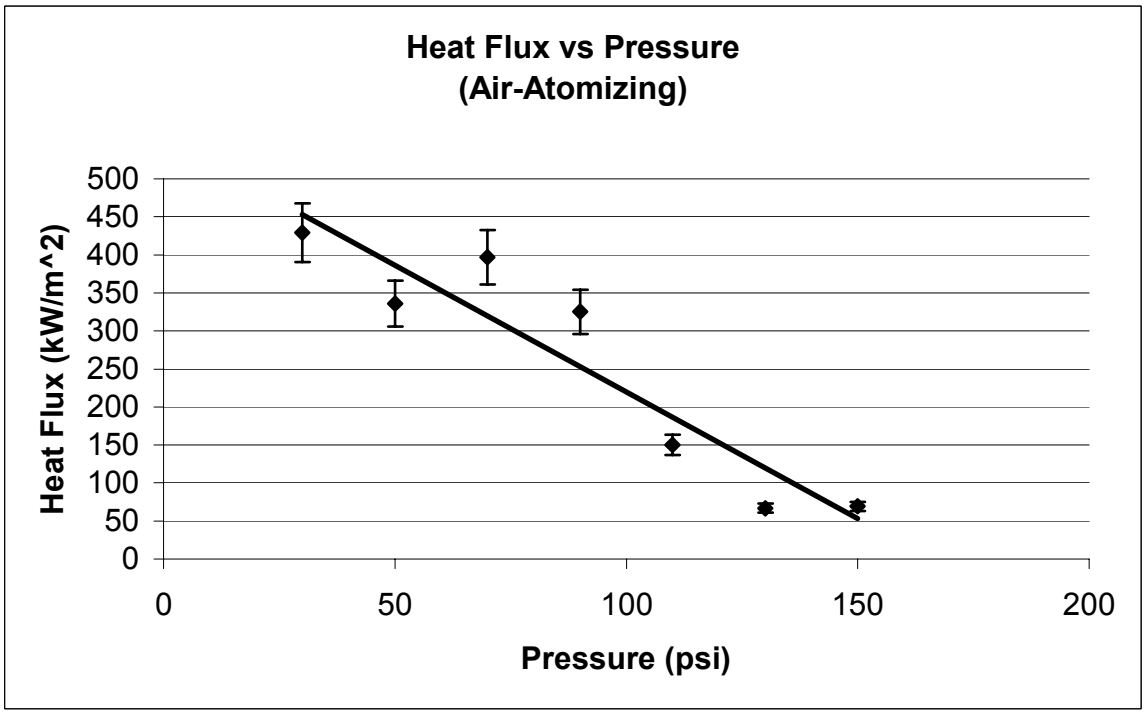


**Figure 30: Estimated heat flux results for air atomizing nozzle**

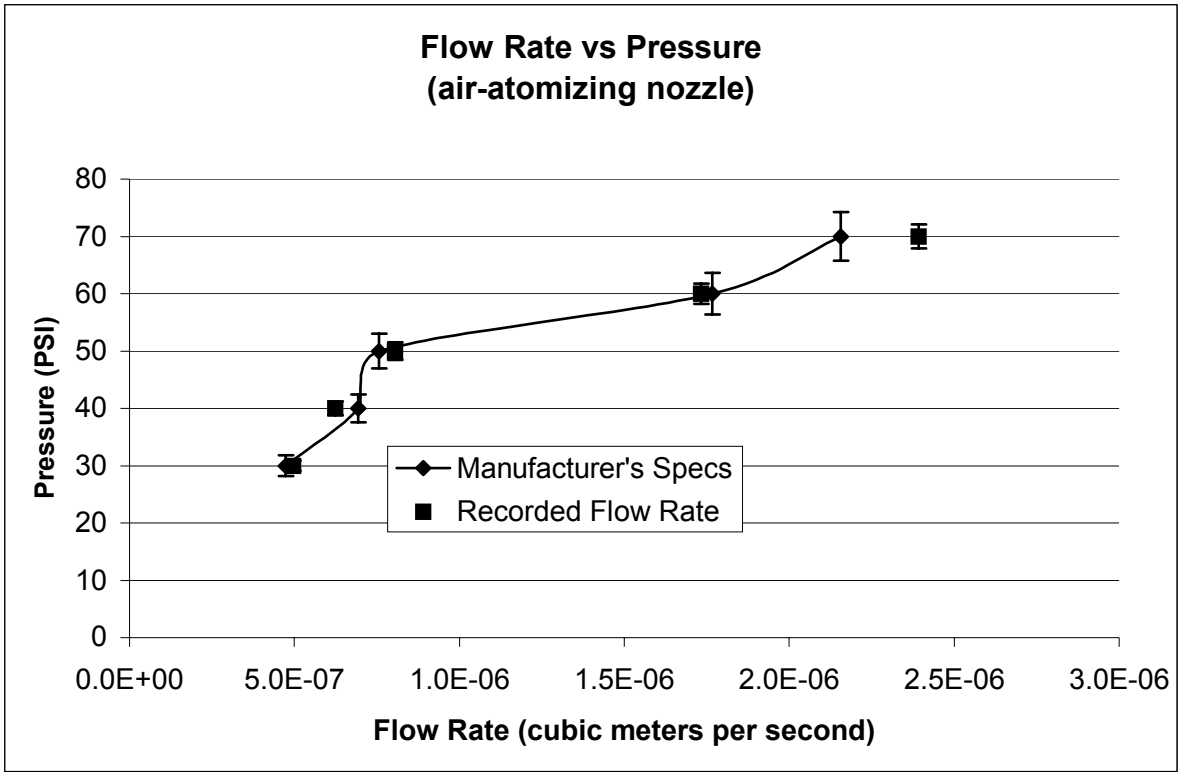


**Figure 31: Theoretical and Actual flow rates for air-atomizing nozzle**

In addition, the air-atomizing nozzle is more uniform in spray characteristics than the water-atomizing nozzle as seen in Figures 32 and 33. This translates into more uniform cooling across the spray cross section at a particular pressure. A uniform spray is preferable to a non-uniform spray because it reduces radial temperature gradients resulting in less stress. Other pressures were not tested due to lab time constraints and lack of compressed air with suitably high pressure.

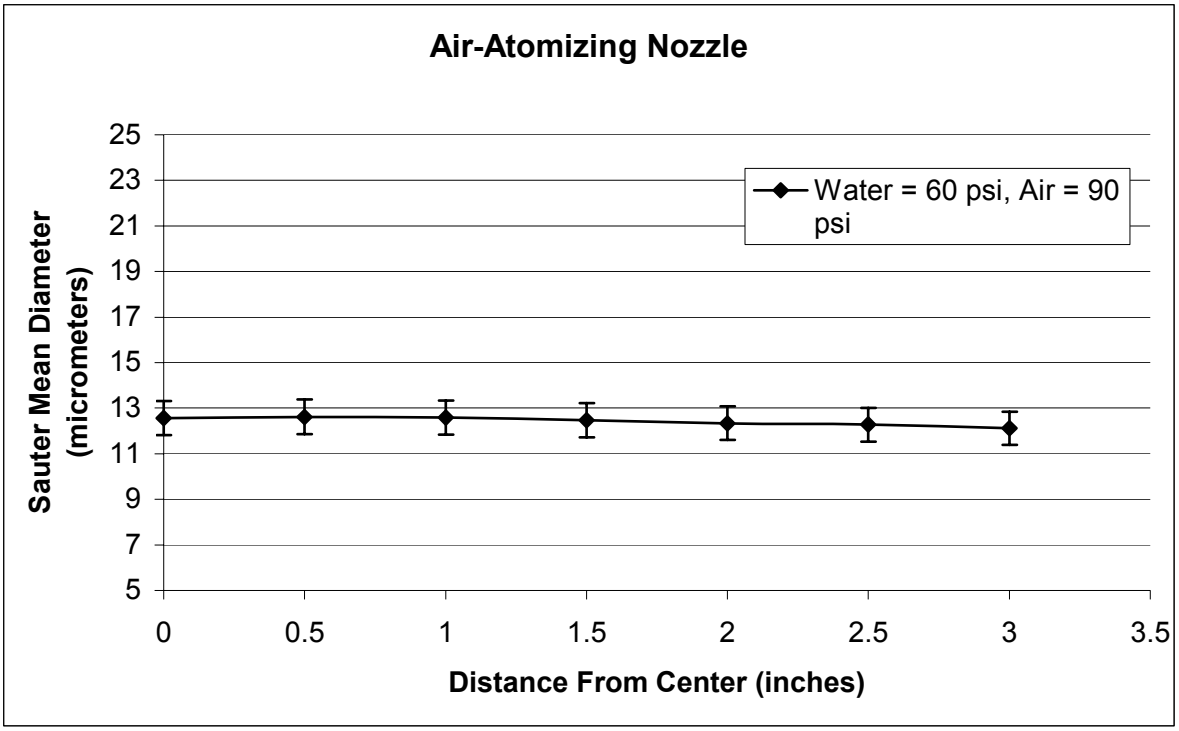


**Figure 32: Sauter Mean Diameter variation from center of spray**

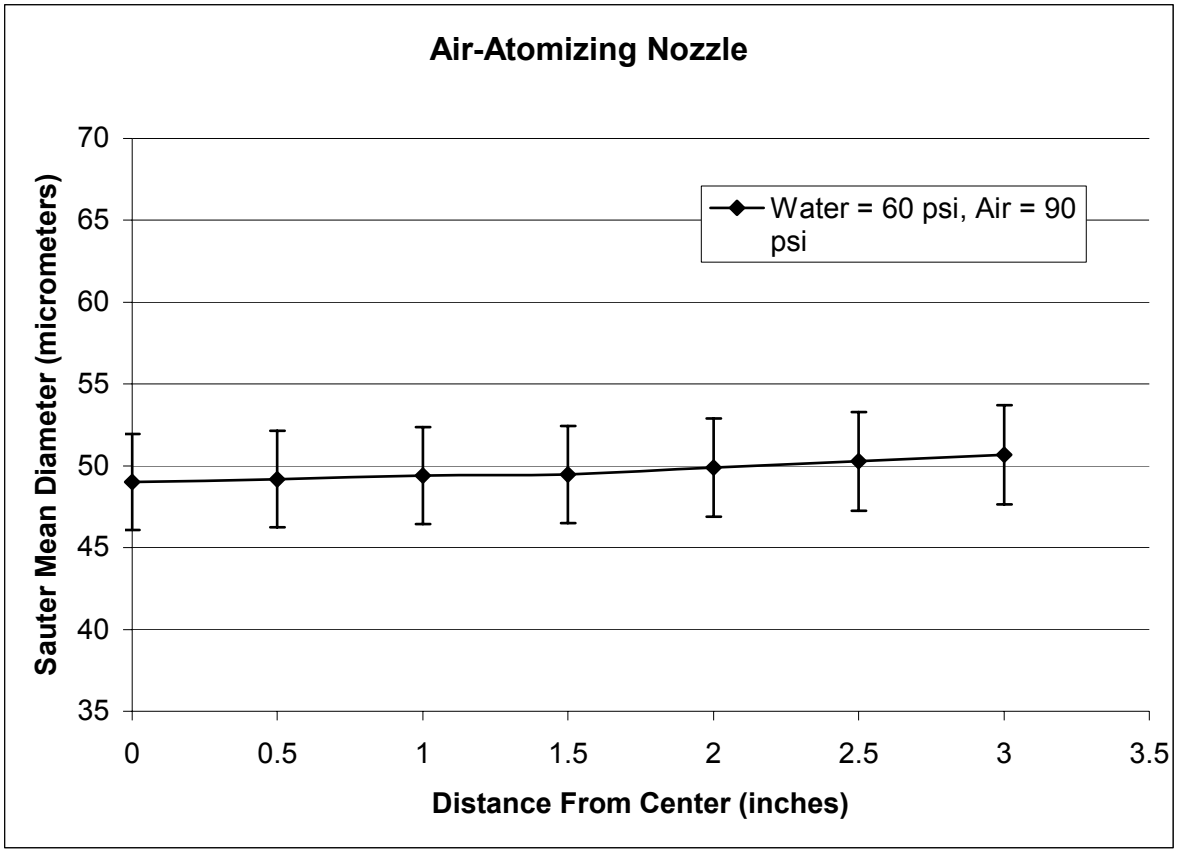


**Figure 33: Average velocity variation from center of spray**

Finally, the Wyman-Gordon nozzle was tested. Due to high turbulence and a random swirling effect in the spray pattern that the nozzle creates, no repeatable results could be recorded. Sauter mean diameter results ranging from 82 microns to 581 microns were recorded. The Sauter mean diameter results were given by the software in a histogram where the entire range was stated. Instead of a steep bell curve as was seen for the both the air atomizing and water-atomizing nozzles, the Wyman-Gordon nozzle produced a flat histogram with recordings in many different size categories. The average reported particle Sauter mean diameter was 361 microns, with a standard deviation of 162 microns. Additionally, the average velocity was anywhere from 6.3 meters per second to 36.1 meters per second and the volumetric spray flux was 0.27 cubic meters per second to 0.118 cubic

meters per second. Because of these varying results, the heat flux could vary greatly from the center to the outer portion of the spray and may vary versus time, unlike the tested nozzles, which are more stable.

## 4.2. Heat Conduction Experiment

The heat conduction experiment provided two pieces of information: the cooling rates and the thermal stresses induced. In Figure 34, the cooling rates at the surface of the test piece are shown for the three tested nozzles, plus a pure air stream.

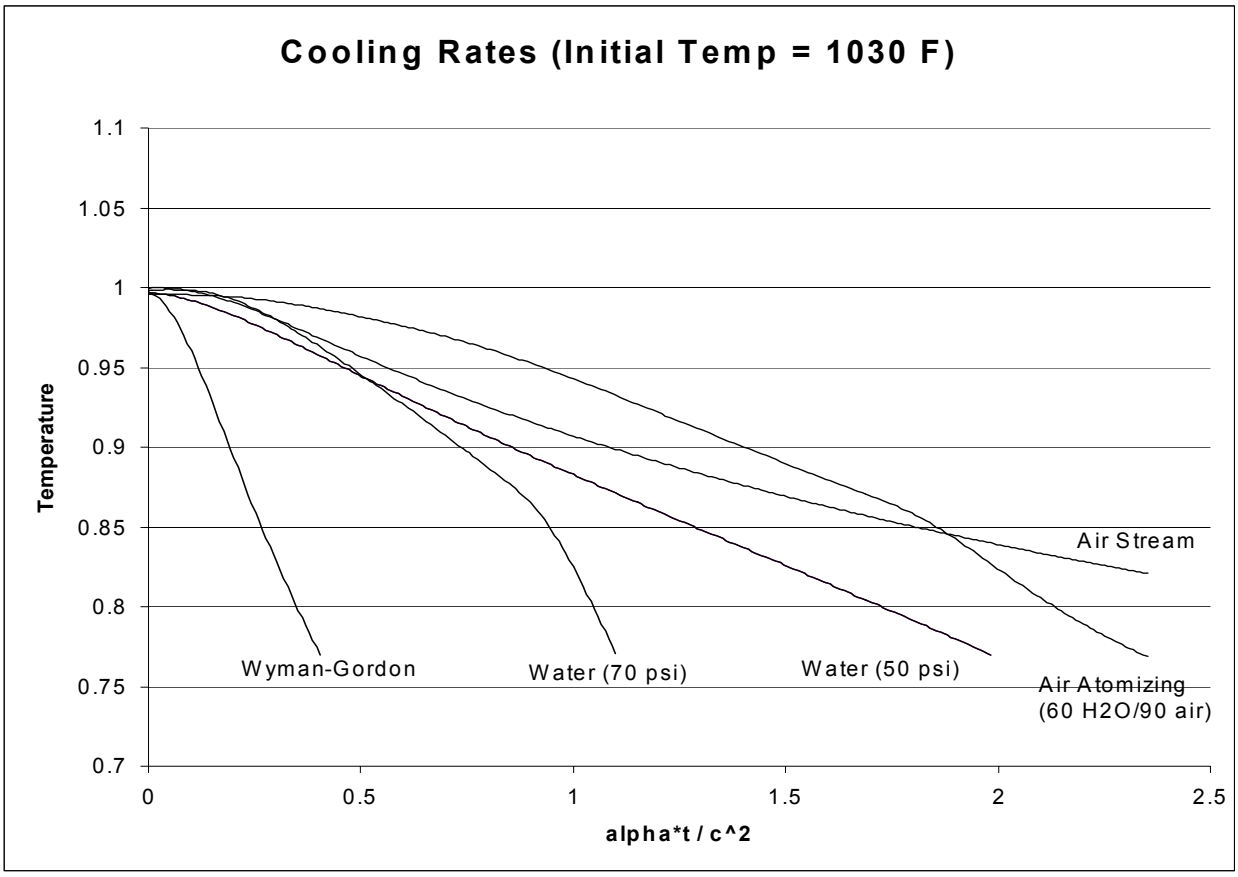


**Figure 34: Cooling rates for the various nozzles**

In Figure 35, the temperature is non-dimensionalized as commonly done in many heat transfer texts. In addition, the time is non-dimensionalized, shown in equation 14.

$$non-dimensional\ temperature = \frac{T_s - T_\infty}{T_i - T\infty} \tag{13}$$

$$non-dimensional\ time = \frac{\alpha t}{c^2} \tag{14}$$

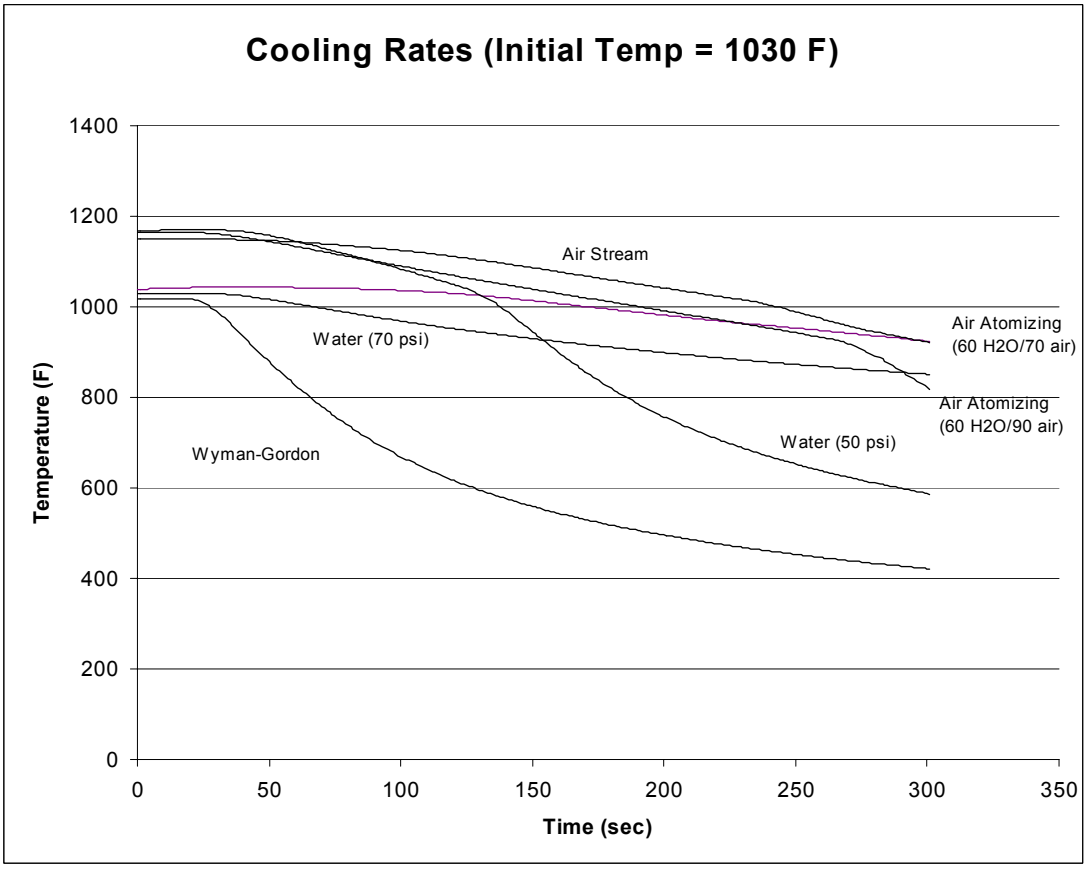


**Figure 35: Actual cooling rates**

As expected, a pure air nozzle creates the lowest cooling rate. The air-atomizing nozzle, regardless of the pressure settings, also produced a low cooling rate, actual cooling times are shown in Figure 34. The water atomizing nozzle and the Wyman-Gordon nozzle, however,

created the fastest cooling rates. Note that the air-atomizing nozzle with the setting of 70 psi for air is not listed because the results are not distinguishable from the other air-atomizing nozzle.

The thermal stresses, calculated using equations 8 to 10, for the three nozzles and air also increased from the pure air jet to the Wyman-Gordon nozzle. Table 2 compares the different test data (the settings are in parentheses). The radial stress, as opposed to the vertical axis stress, is the highest because the sprays did not cover the entire piece. The temperature gradients were higher as one moved out from the center, which induced the higher thermal stresses. Additionally, the radial stress decreases further into the test piece, shown in Figure 36. The thermal stress for the pure air jet does drop, but not as much as the other nozzles. The Wyman-Gordon nozzle comes closest to the ultimate tensile strength and with the error ($\pm$ 12 percent from adding up the actual error contributions in Section 2.0) may actually surpass this value. The remaining values for the other nozzles are within the maximum range.

| | Max Stress (Pa) Radial | Percent of Ultimate Tensile Strength | Max Stress (Pa) z direction | Percent of Ultimate Tensile Strength |
|---|---|---|---|---|
| Air | 1.25 E+11 | 9.82 | 1.10 E+11 | 8.64 |
| Wyman-Gordon | 1.19 E+12 | 93.7 | 1.08 E+12 | 85.3 |
| Water (50 psi) | 1.01 E+12 | 79.3 | 8.30 E+11 | 65.2 |
| Water (70 psi) | 1.07 5E+12 | 83.5 | 8.63 E+11 | 67.8 |
| Air/Water Mix (50 psi / 60 psi) | 5.85 E+11 | 45.8 | 4.04 E+11 | 31.7 |
| Air/Water Mix (90 psi / 60 psi) | 7.55 E+11 | 59.2 | 6.42 E+11 | 50.3 |

**Table 2: Thermal Stress for Air and Nozzles**

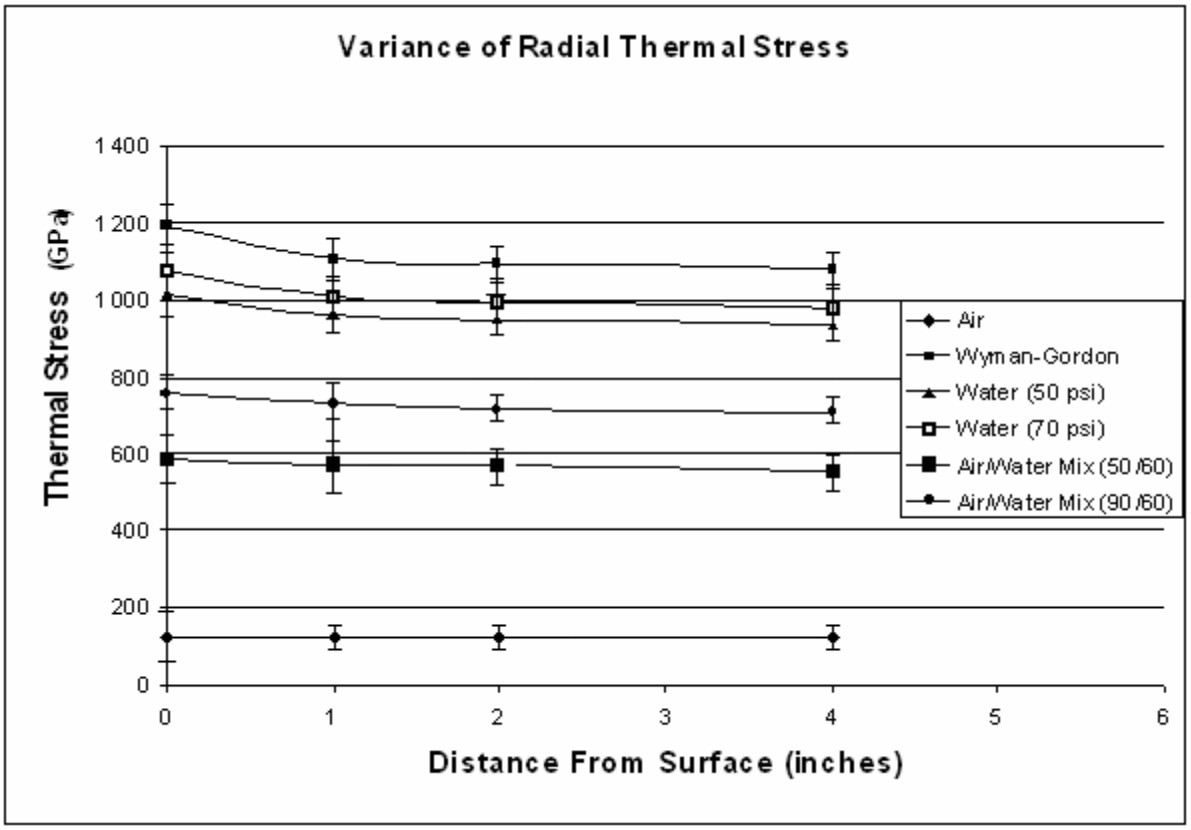


**Figure 36: Radial stress variance as a function of the distance from the surface**

Appendix A shows photographs of the Wyman-Gordon nozzle being tested. Since the nozzle sprays much more water than the other two, one can imagine that the cooling rates should be higher. Engineers at Wyman-Gordon have hypothesized that having so much water pooling in the valleys of the die, that when the hot metal piece is placed on the die and pressed, the water evaporates and causes more stress as it tries to escape. In Appendix B and C respectively, the air-atomizing and water nozzles are tested. All droplets that impact the surface are evaporated off for the air-atomizing nozzle for all times, which may help eliminate this problem. The droplets for the water nozzle are also all evaporated, until a point where the test piece is cool enough on the surface to allow for a pooling of the water. It is surmised that this point is also the approximate operating temperature specified by

Wyman-Gordon. One can see the impacting of the droplets as they begin to "wet" the surface in the center of the test piece. The impacted area appears darker than the rest of the surface. Also, note that since the two pictures in Appendix B and C are taken at around 15 second intervals, the impacted area grows with time.

Calculating a heat flux as described in Section 1.3 provides interesting and necessary data for comparison to previous research. The calculated heat flux values for all the nozzles reached an asymptotic value. This asymptotic value was close to the estimated heat flux as calculated in the Liu paper, for both the air atomizing nozzle and water atomizing nozzles. Figure 37 shows the heat flux value increasing until it reaches about 350 $kW/m^2$. For both air-atomizing nozzle heat flux graphs (the rest are in Appendix D), the heat flux actually increases to the final value. The hot buoyant air or water vapor from the spray may insulate the test piece by keeping the lower momentum particles from impacting the surface.

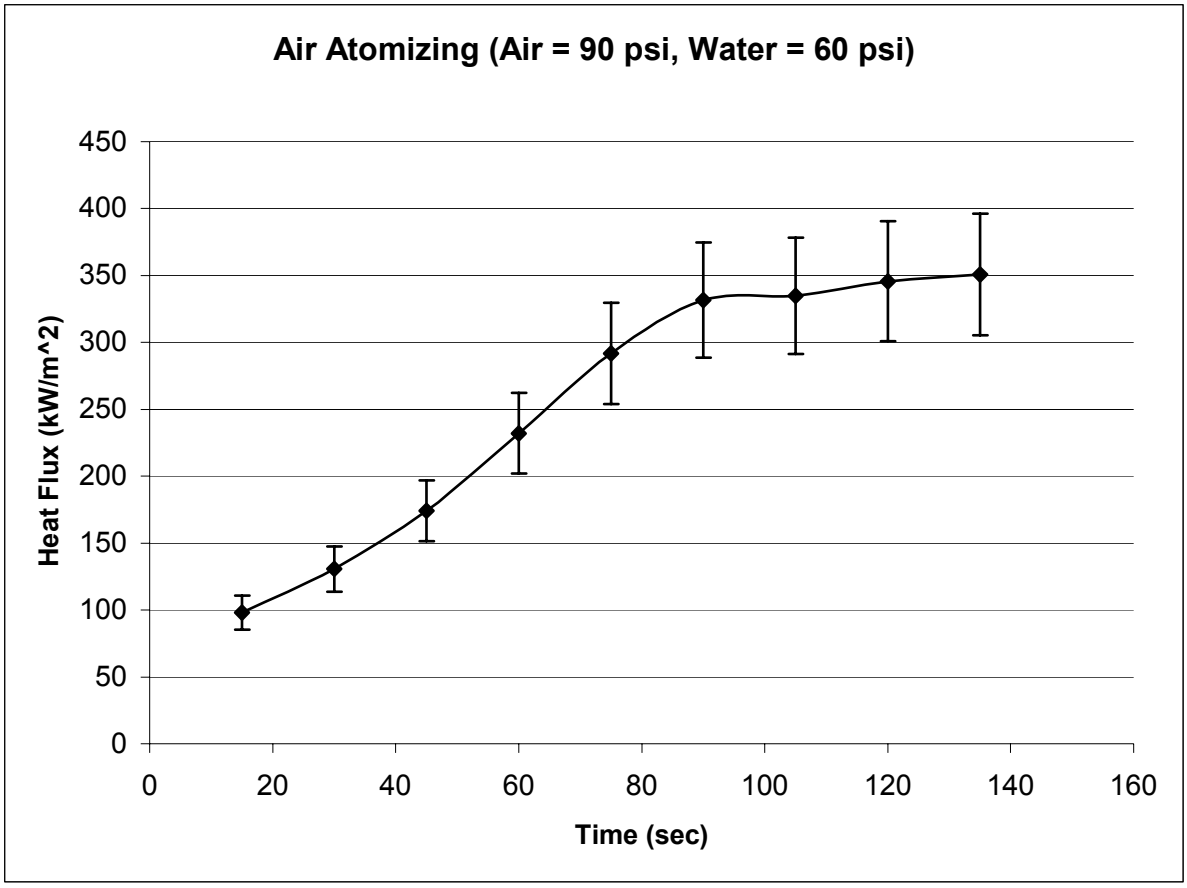


**Figure 37: Experimental heat flux for air-atomizing nozzle at surface (z=0), (air = 90 psi, water = 60 psi)**

A decrease in heat flux was observed for both of the water atomizing nozzles. In Figure 38, the heat flux decreased to its asymptotic value for the 70 psi experiment, except for a small dip in at the beginning of the experiment. This dip is evident in both water atomizing nozzle experiments (Appendix D).

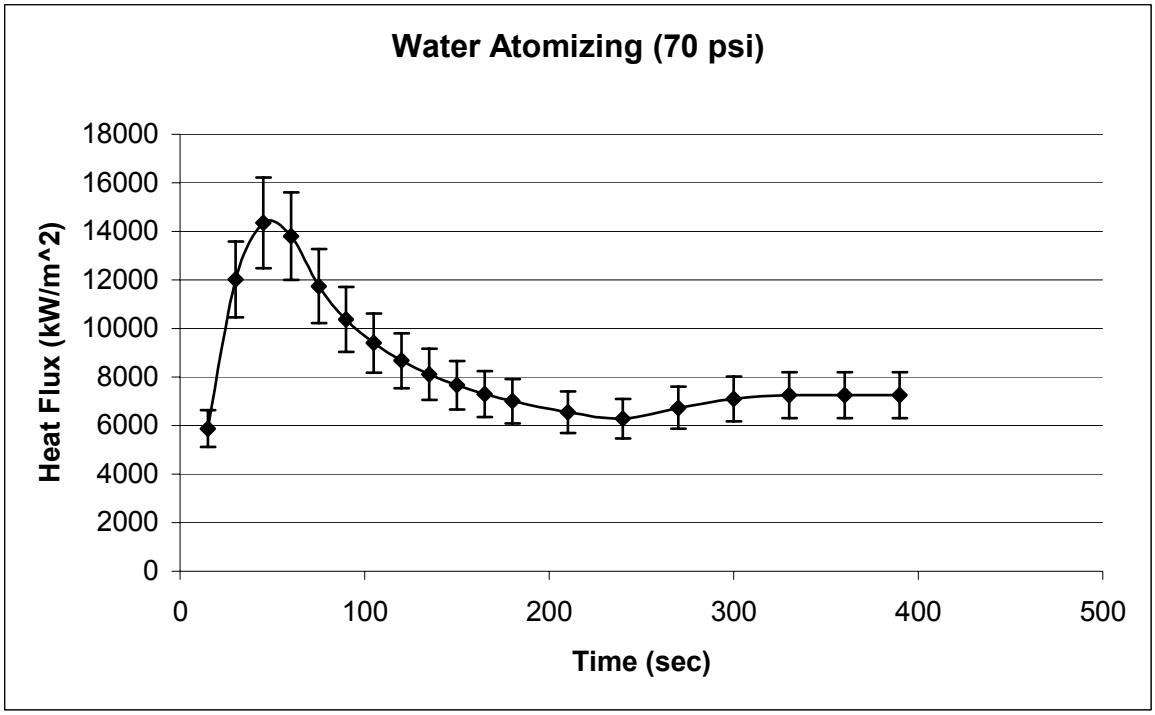


**Figure 38: Experimental heat flux for water atomizing nozzle (70 psi)**

Finally, the Wyman-Gordon heat flux was calculated for the test period (Figure 39). This heat flux had a very large range (0—24000 kW/m$^2$) from beginning to end of test. This supports the idea of high flow rates causing the greatest cooling, since the Wyman-Gordon nozzle had the highest flow rates, and so had the highest heat flux. The graph is irregular and asymptotes at 1000 kW/m$^2$, probably because the test piece has cooled off significantly from its initial temperature.

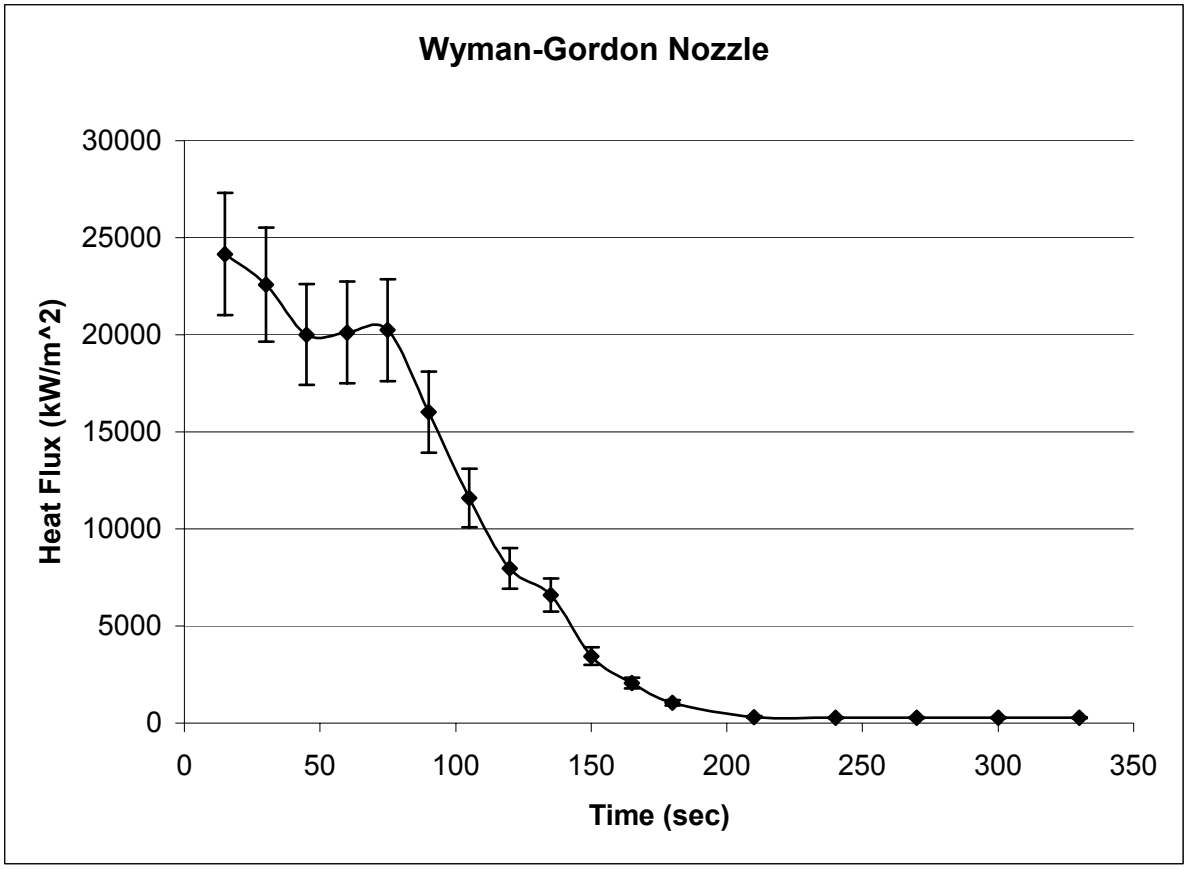


**Figure 39: Experimental heat flux for Wyman-Gordon nozzle**

# 5.0. Discussion and Conclusions

The relationship between the flow parameters, heat flux and thermal stress is very complex, and no definitive correlation exists. Based on the data presented, spray cooling is most sensitive to the volumetric spray flux. The spray flux is followed by the particle size then particle velocity in importance to thermal stress. Numerous reasons can be attributed to this observation. When dealing with high temperatures, around 1000$^{o}$ F (538$^{o}$ C), the buoyant air from the hot metal and/or water vapor from the evaporating droplets becomes an insulator, not allowing low momentum particles to impact the surface. During the testing of the air-atomizing nozzle, this effect became more apparent. A few times, one could see a "wave" of droplets that would send some particles upward. These particles around the outside of the spray pattern probably did not have sufficient vertical momentum to travel through the hot buoyant air and water vapor. The few particles that did penetrate contributed to cooling the piece, and as the temperature dropped, more particles were able to penetrate further cooling the piece. The heat flux graph and the photos support this idea. In Figure 37, the heat flux actually increases, suggesting that the surface was initially being insulated by the hot buoyant air, until more droplets impacted the surface, causing a higher heat flux. This increase can be attributed to the impacting of the water droplets onto the surface, evident in Appendix B where one can see the wetted area increasing. Even with the water atomizing nozzles, the wetted area increased causing the increase and eventual decrease in the heat flux. Due to the fact that the heat flux decreases with the increase of pressure and the increase of the volumetric spray flux, if the volumetric spray flux is the same as the

Wyman-Gordon nozzle, the water nozzle would probably cool less than the Wyman-Gordon nozzle. The insulation of the test piece by buoyant air was also observed when the nozzle was being set up and the test piece was beginning to reheat from the last test. When the air-atomizing nozzle was turned on, the die test piece was cool (only around 450° F or 232° C), and the temperature dropped when the spray was applied. Although the drop in temperature was promising, at the high temperatures this did not occur leading to the conclusion that the momentum of the particles must play a more important role.

Liu [2] predicts that the heat flux should decrease with time for the range of conditions considered in this thesis. All the nozzles do indeed follow this trend except for the air-atomizing nozzle for reasons discussed earlier. Liu also predicts that the volumetric spray flux would be the largest factor in determining the heat flux, followed by the Sauter mean diameter, then particle velocity. This trend was the case in the experiments, however the volumetric spray flux seemed to have a greater influence than in the Liu experiment. In his experiment, the heat flux versus time graph did not take the shape of the volumetric spray flux. This was the case in the present experiments. Whatever the shape of the volumetric spray flux, the heat flux seemed to follow the same shape. The reason for this difference may be due to the different flow regime (higher diameters and velocities) tested in this experiment. The amount of particles that impact the surface may be more significant at higher Sauter mean diameter values and / or velocities than at lower velocities and / or Sauter mean diameter values.

The Wyman-Gordon process of cooling using the current nozzle was also of interest. Although one cooling rate was obtained in the results, it is important to note that since the Wyman-Gordon nozzle produced a very turbulent, inconsistent spray, the actual cooling rates

within the spray could vary greatly. There is a large difference in heat flux of 24000 $kW/m^2$ between the start and end of the Wyman-Gordon nozzle experiment. Any number of factors could contribute to this, including the varied flow parameters and the fact that the test piece had cooled very quickly. This high cooling rate, plus the variance in the spray parameters, would lead to high thermal gradients within the test piece causing high thermal stress and cracking at the surface. The surface crack problem would then be compounded and worsened by the load stresses in the dies during operation. Note that although the cooling problem is not the only contribution to the problem of cracking die, it is considered a major contributor.

# 6.0. Recommendations

Based upon the results, two courses of action should be pursued. First, in the short term, the current Wyman-Gordon nozzle should be replaced with a more consistent spray nozzle, preferably the water nozzle at around 50 to 70 pounds per square inch. The reason for this is because the water nozzle is capable of producing a more even spray and can produce the same amount of temperature reduction as the current Wyman-Gordon nozzles do in 20-30 seconds. The water nozzle should be applied for about 60 to 75 seconds, 1.2 times longer than the current 40 second application time, or stopping when the water begins to pool on the surface. An increase in the flow rate of the water-atomizing nozzle would also produce faster cooling rates, possible reducing the application time. The second recommendation, in the longer term, is a cooling method, such that the spray is being applied evenly to the entire die surface as opposed to area cooling as is done currently, would be devised. The fact that the radial stress is greater than the axial stress suggests that if the piece is cooled evenly, the radial stress (the higher of the two stresses) is lessened. Due to the immense size, the spraying system may consist of an oscillating head configuration should be devised to ensure a larger area of cooling.

## References


[1] Allsop, D.G. Kennedy, D. Pressure Diecasting. Pergamon Press, 1983.

[2] Kaye, A. Street, A. Die Casting Metallurgy. Butterworth Scientific, 1982.

[3] Schick, Rudolf, An Engineer's Practical Guide to Drop Size. Spraying Systems Co., 2000.

[4] Liu, G.W., Morsi, Y.S., Clayton, B.R. Characterisation of the Spray Cooling Heat Transfer Involved in a High Pressure Die Casting Process. International Journal of Thermal Science 39 (2000) 582-591.

[5] Schmidt, J., Boye, H. Influence of Velocity and Size of the Droplets on the Heat Transfer in Spray Cooling. Chemical Engineering Technology 24 (2001) 255-260.

[6] Pasandideh-Fard, M., Aziz, S.D., Chandra, S., Mostaghimi, J. Cooling Effectiveness of a Water Drop Impinging on a Hot Surface. International Journal of Heat and Fluid Flow 22 (2001) 201-210.

[7] Tartarini, P. Lorenzini, G. Randi, M.R. Experimental Study of Water Droplet Boiling on Hot, Non-Porous Surfaces. International Journal of Heat and Mass Transfer 39 (1999) 437-447.

[8] Thomas, R., Ganesa-Pillai, M., Aswath, P.B., Lawrence, K.L., Haji-Sheikh, A. Analytical/Finite Element Modeling and Experimental Verification of Spray Cooling Process in Steel. Metallurgical and Materials Transactions A 29A (1998) 1485-1498.

[9] Chen, R.H., Chow, L.C., Navedo, J.E. Effects of Spray Characteristics on Critical Heat Flux in Subcooled Water Spray Cooling. International Journal of Heat and Mass Transfer, April 2002.

[10] Bejan, A. Heat Transfer. John Wiley and Son Inc., 1993.

[11] Tong, L.S. Boiling Heat Transfer and Two-Phase Flow. John Wiley and Son Inc., 1965.

[12] Beck, J. Blackwell, B. St. Clair Jr., Charles R. Inverse Heat Conduction. Wiley-Interscience Publication, 1985.

[13] Gatewood, B.E. Thermal Stresses. McGraw Hill Publications, 1957.

# Appendix A

**Figure 41: Wyman-Gordon nozzle inverse heat conduction test**

# Appendix B

**Figure 41: Air-Atomizing nozzle inverse heat conduction test**

**Figure 42: Air-Atomizing nozzle inverse heat conduction test (15 seconds later)**

# Appendix C

**Figure 43: Water atomizing nozzle inverse heat conduction test**

**Figure 44: Water atomizing inverse heat conduction test (15 seconds later)**

# Appendix D

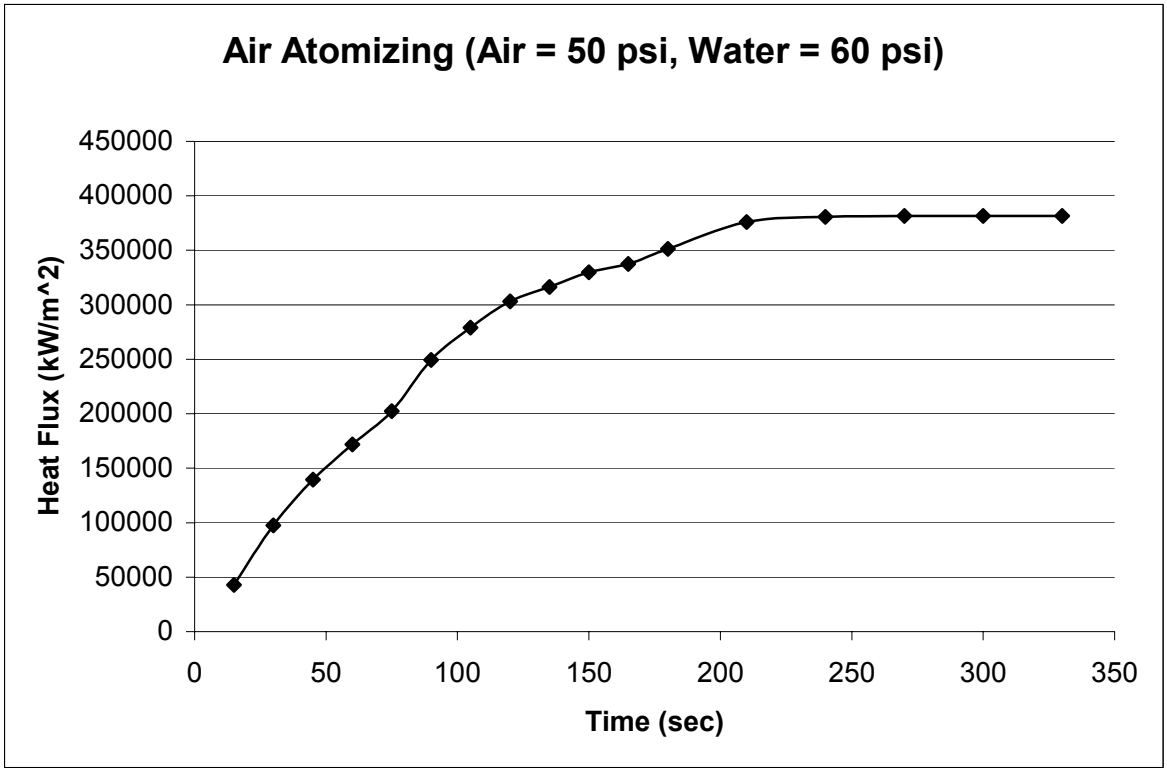
Air Atomizing (Air = 50 psi, Water = 60 psi)
Heat Flux (kW/m^2)
450000
400000
350000
300000
250000
200000
150000
100000
50000
0
0
50
100
150
200
250
300
350
Time (sec)

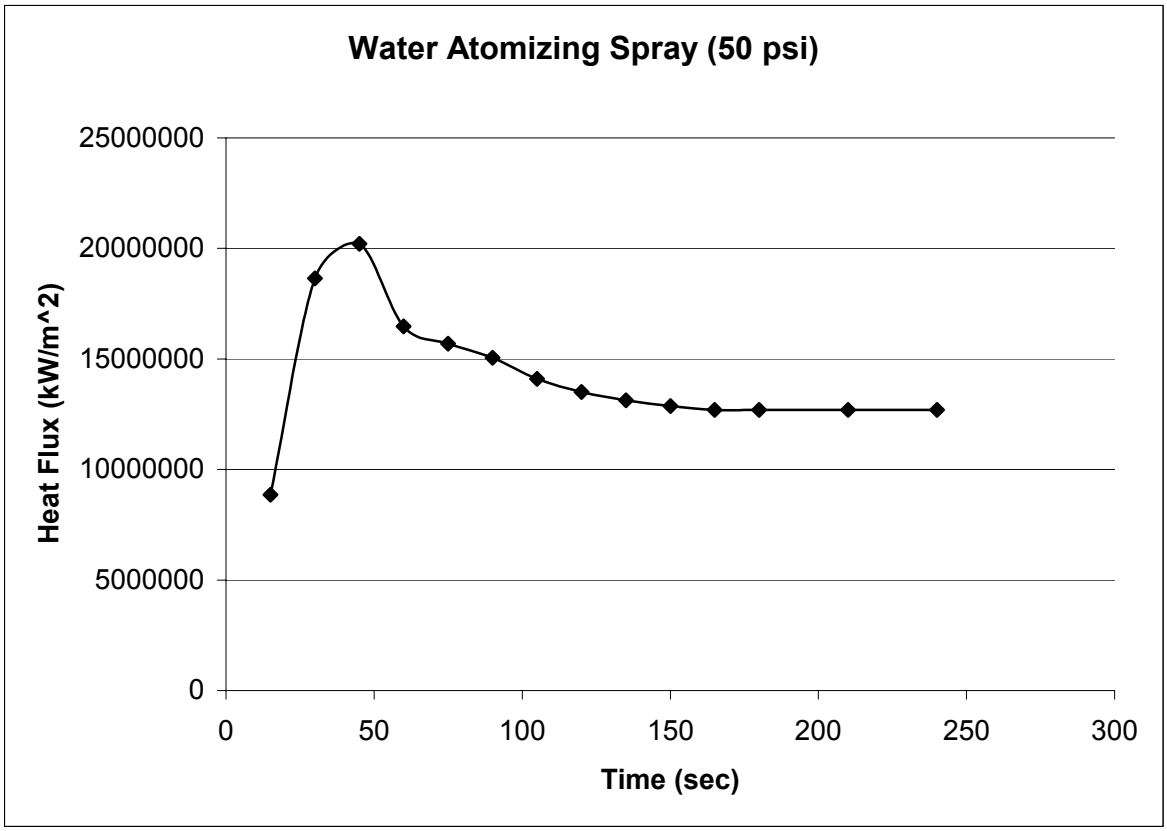
Water Atomizing Spray (50 psi)
Heat Flux (kW/m^2)
25000000
20000000
15000000
10000000
5000000
0
0
50
100
150
200
250
300
Time (sec)